ACS OMEGA

Open Access

http://pubs.acs.org/journal/acsodf

Article

Rhoifolin Attenuates Concanavalin A-Induced Autoimmune Hepatitis in Mice via JAKs/STATs Mediated Immune and Apoptotic Processes

Ge Zhao, Hu Qi, Minghua Liu, Ting Zhou, Li Chen, Chunhong Wu, Xiongwei Zhang, Nan Zeng,* and Yue Tong*

Cite This: *ACS Omega* 2024, 9, 43233−43251

Read Online

ACCESS | Metrics & More | Article Recommendations

ABSTRACT: Rhoifolin (ROF) exhibits a diverse range of biological activities, encompassing anticancer, hepatoprotective, antidiabetic, antirheumatic, and antiviral properties. However, the specific protective effects and possible mechanisms of the compound against T-cell-mediated autoimmune hepatitis have not been previously elucidated. In the present study, adult male mice were administered Con A (20 mg/kg, intravenously) for 8 h. In the treated groups, mice were pretreated with ROF daily (20 mg/kg and 40 mg/kg, orally) for 7 days before Con A intoxication. The results showed that ROF significantly decreased serum biochemical indices (ALT, AST, ALP, and LDH) and regulated related oxidative stress indicators (MDA, SOD, and GSH), reduced hepatic necrosis areas and immune cells infiltration, inhibited the release of various inflammatory factors (TNF-α, IFN-γ, IL-2, and IL-17), and improved hepatic tissue apoptosis, thereby alleviating hepatic damage induced by Con A. Additionally, we have also confirmed that ROF efficiently inhibited Th1/Th17 cells polarization via modulation of the JAK2/JAK3/STAT1/STAT3 signaling pathways both *in vivo* and *in vitro*. Moreover, the molecular mechanism examination also demonstrated that ROF regulated apoptotic cascade signaling through IL-6/JAK2/STAT1/STAT3 controlling BNIP3 activity in primary hepatocytes. These effects were in good agreement with the bioinformatics analysis of ROF treatment for AIH. In conclusion, our findings provide new insights into the potential use of ROF for AIH therapy, which may result from the specific regulation of the T cell subtype polarization and the apoptosis of liver cells via modulation of the JAKs/STATs signaling pathways.

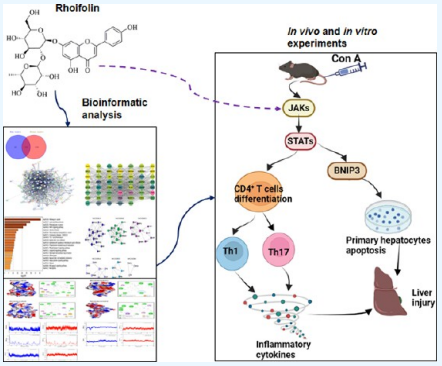

1. INTRODUCTION

Autoimmune hepatitis (AIH) is a severe inflammatory liver condition characterized by acute onset, rapid advancement, and a high fatality rate, affecting individuals across various demographic groups.[1] The morbidity of AIH is commonly linked to various factors, including genetic susceptibility, environmental influences, hepatitis viruses, drug-induced reactions, and others.[2] The primary pathological presentation of AIH involves significant necrosis and apoptosis in the liver. These processes not only result in a rapid deterioration of activity function but also ultimately lead to the development of more severe conditions such as hepatic cirrhosis and failure in the absence of appropriate treatment.[3] To date, the specific etiology of AIH is not fully understood, and immunosuppressive agents and liver transplantation are the primary available treatments for AIH.[4] For example, the standard clinical protocol for managing AIH typically includes the administration of corticosteroids and azathioprine, which has demonstrated the ability to achieve disease remission in 80−90% of patients.[5] As far as we know, the use of steroids and azathioprine has been associated with a variety of side effects that necessitate thorough evaluation and consideration. Moreover, liver transplants face limitations due to factors such as a shortage of donors, the need for immunosuppression, and the high expenses involved.[6] Hence, there is an urgent and critical need to develop safe and efficacious medications for patients suffering from AIH.[7]

Concanavalin A (Con A), a plant lectin purified from the jack beans (*Canavalia brasiliensis*), is commonly employed to induce and develop the models of hepatic injury for acute immune-regulated hepatitis, which strikingly resemble the pathogenic pathways and pathological changes seen in viral hepatitis or AIH patients.[8] Multiple reports have indicated that the activation and mobilization of T cells to the liver are

Received: August 28, 2024
Revised: September 27, 2024
Accepted: October 3, 2024
Published: October 11, 2024

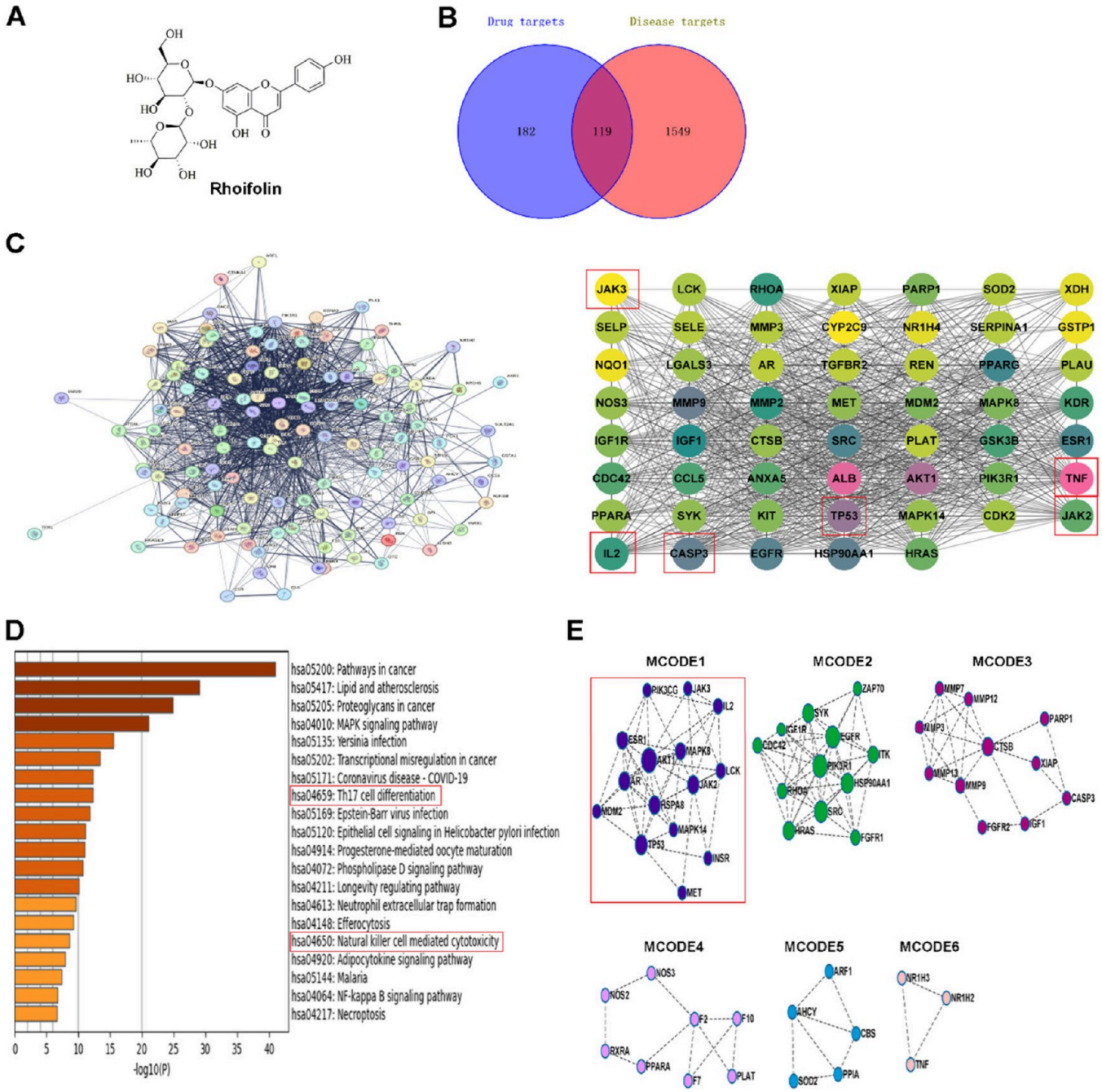

Figure 1. Bioinformatics analysis of ROF against AIH (A) The structure of ROF. (B) Venn diagram comparing the targets of ROF and AIH. (C) PPI network construction and identification of core targets. (D) KEGG enrichment analysis. (E) MCODE analysis for the PPI network.

responsible for the development of Con A-induced acute hepatitis.[9] Upon intravenous administration of Con A in mice, $CD4^+$ T cells in both the peripheral and the intrahepatic compartments were activated. For instance, T helper 0 (Th0) cells are activated upon recognizing the MHC class II-Con A complex through their T cell receptor (TCR), subsequently differentiating into several Th subtypes including Th1, Th2, Th17, and regulatory T cells (Treg). Particularly, Th1 cells can produce interferon (IFN)-γ and tumor necrosis factor (TNF)-α, whereas Th17 cells generate interleukins (IL)-17 and IL-22.[10] Prominently, these secreted proinflammatory cytokines play a significant role in influencing and recruiting other immune cells, including Kupffer cells, neutrophils, eosinophils, and natural killer T (NKT) cells, to infiltrate and accumulate within liver tissue, thereby contributing to hepatic damage through both direct and indirect mechanisms.[11] Additionally, recent research has also indicated that although $CD8^+$ T cells do not have a direct association with Con A, their activation is believed to be triggered by the Con A-regulated production of TNF-α and IFN-γ. Consequently, $CD8^+$ T cells are involved in the induction of apoptosis in hepatocytes through the Fas/FasL pathway.[10]

The Janus kinases (JAKs)/signal transducer and activator of transcriptions (STATs) signaling pathways, which play important functions in immunological regulation, cellular differentiation, hematopoiesis, and metabolic processes, represent a conserved signaling mechanism across evolutionary development.[12] The JAKs/STATs signaling pathway is canoni-

https://doi.org/10.1021/acsomega.4c07915
ACS Omega 2024, 9, 43233−43251

cally enabled when cytokines interact with their corresponding receptors, leading to a conformational change that facilitates the recruitment of associated JAKs. The phosphorylation of JAKs subsequently induces the tyrosine phosphorylation of the receptors, thereby creating docking sites for their related downstream signaling molecules, STATs. Upon phosphorylation, STATs dissociate from the receptor, translocate to specific DNA sequences, and regulate the transcription of genes associated with cytokines by entering the nucleus as either homodimers or heterodimers.[13] Various research studies have demonstrated the substantial influence of cytokine-induced activation of JAKs/STATs pathways on hepatic damage connected to AIH and the differentiation and maturation of immune cells.[14,15] For instance, activation of STAT1 and STAT4 is induced by IFN and IL-12, respectively. This activation leads to the upregulation of *T-bet* gene expression, which is crucial for the differentiation of Th1 cells. Similarly, IL-4 accelerates Th2 cell differentiation by upregulating GATA-binding protein-3 (*GATA3*) gene expression through STAT6. In contrast, Th17 cells differentiation relies on the presence of transforming growth factor (TGF) and IL-6, which act through STAT3 to stimulate retinoic acid-related orphan receptor-γt (*RORγt*) gene expression.[12] For the apoptotic processes in hepatic tissues in AIH, the activation of STAT1 by IFN-γ leads to hepatocytes death. Particularly, upon stimulation by IFN-γ, STAT1 enables the formation of homodimers, which then bind to the IFN-γ activated sequence located on the promoter and finally trigger the heightened production of chemokines, adhesion molecules, and reactive oxygen species (ROS).[14] Studies have reported that mutant mice that overexpress STAT1 exhibit increased IFN-γ levels and experience exacerbated hepatic damage following Con A injection. Conversely, STAT1-deficient (STAT1−/−) animals show reduced liver damage in response to Con A.[14] Additionally, the binding of IL-6 to its receptor activates JAK kinases, specifically JAK1 and JAK2, which facilitate the STAT3 phosphorylated, resulting in STAT3 dissociation, dimerization, and translocation to the nucleus.[15] Phosphorylated STAT3 functions as a transcription factor that upregulates the expression of many target proteins, including Bcl-2/adenovirus E1B 19 kDa interacting protein 3 (BNIP3). BNIP3 has the capacity to interact with Bcl-2, thereby reducing the antiapoptotic effects of Bcl-2 and ultimately facilitating the process of apoptosis.[16] Therefore, the dual regulation of T cell adaptive immune responses and hepatocyte apoptosis by JAKs/STATs can serve as important molecular pathway targets for hepatic damage therapy in the AIH model.

Rhoifolin (ROF), also referred to as apigenin 7-*O*-β-neohesperidoside, is a glycoside belonging to the flavonoid class, specifically within the apigenin family.[17] It was extracted from a diverse range of botanical sources, including *Rhus* species, artichokes, tomatoes, etc. Furthermore, it was found in large quantities in several sections and juices of many *Citrus* spp.[18] Several investigations have demonstrated that this flavone glycoside has a broad spectrum of biological actions, including antitumor, antioxidant, hepatoprotective, anti-inflammatory, and antiviral properties.[17] For example, ROF derived from Plumula Nelumbinis exerts an inhibitory effect on pancreatic cancer through the modulation of the protein kinase B (AKT)/c-Jun N-terminal kinase (JNK) signaling pathways.[19] ROF also has the capability to mitigate osteolysis and osteoclastogenesis induced by titanium particles via regulating the receptor activator of nuclear factor-κB ligand (RANKL)-mediated nuclear κ-light-chain-enhancer of activated B cells (NF-κB) and mitogen-activated protein kinase (MAPK) signaling pathways.[20] Moreover, ROF mitigates alcoholic liver disease both *in vivo* and *in vitro* through the inhibition of the toll-like receptor 4 (TLR4)/NF-κB signaling pathway.[21] However, currently, whether ROF possessed the potential to modulate the immune system in order to protect the liver against AIH-induced hepatic damage still remains unclear. Hence, the objective of this research was to explore the preventative benefits of ROF and possible mechanisms using a series of both *in vitro* and *in vivo* experimental studies.

2. MATERIALS AND METHODS

2.1. Chemicals and Reagents. Rhoifolin (ROF, no. PHL83302, as depicted in Figure 1A) and tofacitinib (TOF, no. PZ0017) were obtained from Sigma-Aldrich (St. Louis, MO, United States). Con A (#T4004) was acquired from Topscience (Shanghai, China). Anti-CD4 (#ab183685) and anti-IL6 (#ab290735) were purchased from Abcam (Cambridge, U.K.). The FITC-conjugated anti-mouse CD3 (#553061), BV510-conjugated anti-mouse CD4 (#563106), BB700-conjugated anti-mouse CD4 (#566407), BV421-conjugated anti-mouse IFN-γ (#563376), leukocyte activation cocktail with BD GolgiPlug (#550583), and fixation/permeablization kit (#554714) were acquired from BD Biosciences (CA, USA). PE-conjugated IL-17A (eBio17B7) (#12-7177-81) was obtained from eBioscience (CA, USA). Anti-mouse Ly-6G was obtained from Proteintech (Wuhan, China). Anti-Bax (#T40051) and anti-Bcl-2 (#T40056) were sourced from Abmart (Shanghai, China). Additionally, the antibodies specific to cleaved caspase-3 (#9664), cleaved caspase-9 (#9509), JAK2 (#3230), JAK3 (#8863), and BNIP3 (#3769) were obtained from Cell Signaling Technology (MA, USA). STAT1 (#AF6300), p-STAT1 (#AF3300), STAT3 (#AF6294), p-STAT3 (#AF3293), p-JAK2 (#AF3024), and p-JAK3 (##AF8160) were provided by AFFINITY (Wuhan, China). Percoll (#BS909) and hematoxylin and eosin (H&E) (#BL700A) were procured from Biosharp (Hefei, China). Bifendate pills (BIF, #UF40010) were acquired from Baiyunshan Xingqun Pharmaceutical (Guangzhou, China).

2.2. Bioinformatics Analysis. *2.2.1. Target Acquisition of ROF against AIH.* The potential targets of ROF and AIH were identified through an analysis of various databases. Specifically, in databases such as TCMSP (https://www.tcmsp-e.com/#/database), Swiss target prediction (http://www.swisstargetprediction.ch/), and PharmMapper (http://www.lilab-ecust.cn/pharmmapper/), drug targets associated with ROF were gathered, and a comprehensive review of relevant literature was conducted to match gene names. Moreover, disease targets related to AIH were collected from databases including Gene Cards (https://www.genecards.org/), OMIM (https://omim.org/), and TTD (https://db.idrblab.net/ttd/), using the keyword "autoimmune hepatitis". These targets were then integrated and refined to align with the gene names. The Venny 2.1 tool was employed to ascertain the intersection between the ROF and AIH targets.

2.2.2. Protein−Protein Interaction (PPI) Network Construction and Core Target Analysis. The identified target genes, which are common to both drug targets and disease targets, were uploaded into STRING 12.0 (https://cn.string-db.org/). The species was designated as "Homo sapiens", and the anticipated protein−protein interactions (PPI) were derived from an online network analysis. The results were

https://doi.org/10.1021/acsomega.4c07915
ACS Omega 2024, 9, 43233−43251

subsequently imported into Cytoscape version 3.10.0 in TSV format for core target analysis using the Centiscape 2.2 plug-in, adhering to the condition that the values of degree centrality, closeness centrality, or betweenness centrality were equal to or exceeded the median.

2.2.3. Kyoto Encyclopedia of Genes and Genomes (KEGG) and Molecular Complex Detection (MCODE) Algorithm. The KEGG enriched ontology clusters were analyzed in the Metascape database (https://metascape.org/). The species was designated as "Homo sapiens", and the visualization of the top 20 KEGG enriched entries was carried out following the sorting of the columns based on the $-\log_{10}$ (p-value) in descending order.

The MCODE algorithm identifies dense regions within a protein network by analyzing the connection patterns. These regions often represent significant complexes or modules involved in biological processes.[22] Consequently, the MCODE algorithm was applied to analyze the PPI network by using Cytoscape software to find neighborhoods with high connectivity, resulting in the identification of six clusters (MCODE1−6). The "biological meanings" of each MCODE network were then extracted from the network components through Gene Ontology (GO) enrichment analysis, retaining the top three terms with the most significant p-values.

2.3. Molecular Docking and Dynamic Simulation. The three-dimensional conformer of ROF was obtained from the PubChem database (https://pubchem.ncbi.nlm.nih.gov/), subsequently subjected to energy minimization using Chem 3D software, and converted to the MOL2 format. The protein crystal structures of JAK2 (PDB ID 8BXH), JAK3 (PDB ID 5LWM), STAT1 (PDB ID 3WWT), and STAT3 (PDB ID 6NJS) were obtained from the RCSB Protein Data Bank (https://www.rcsb.org/) and underwent the removal of ligand and water molecules using the PyMOL 2.6 software (Schrödinger, USA). Next, the structures of compound and proteins were prepared utilizing AutoDock Tools 1.5.7 to add hydrogen and saved in PDBQT format. The molecular docking procedure was conducted using AutoDock Vina 1.2.5 (Scripps Research Institute, USA) to study the binding characteristics of the ROF with each of the aforementioned proteins. The ligand exhibiting the lowest binding energy was chosen for further analysis of the binding mode, and the docking results were visualized in three dimensions using PyMOL 2.6 software.

To further study the molecular mechanisms underlying the binding of ROF to the JAK2/3 protein, molecular dynamics simulations were performed on the selected receptor protein−small molecule complexes using GROMACS 2020 software. The protein utilized the AMBER99SB-ILDN force field parameters, while the small molecule ligand employed the GAFF general force field parameters. The topology of the small molecule was constructed using the Sobotop program, and charge fitting was conducted using the RESP method. The TIP3P explicit water model was selected with the minimum distance from the protein atoms to the edge of the water box set at 1.0 nm. Based on the docking results, sodium or chloride ions were added to neutralize the system's charge. The molecular dynamics simulation workflow consists of four key steps: energy minimization, heating, equilibration, and the production of molecular dynamics simulations. First, the heavy atoms of the constrained protein, along with small molecules, underwent 10 000 steps of energy minimization, which included 5000 steps of steepest descent followed by 5000 steps of the conjugate gradient method. After this, the constraints were released, and the entire system experienced an additional 10 000 steps of energy minimization. During the energy optimization phase, the system was gradually heated to 300 K over a period of 50 ps, and equilibration was performed under both canonical (*NVT*) and isobaric-isothermic (*NPT*) ensembles. Finally, the system underwent a 100 ns molecular dynamics simulation within the *NPT* ensemble. Trajectory data were saved every 10 ps, and relevant analyses were conducted using the trjconv module. The binding free energy calculation for the ligand and protein was performed using the g_MMPBSA method from the GROMACS 2020 program.

2.4. Animals and Designing Experiments. SPF Biotechnology (Beijing, China) provided male C57BL/6J mice, aged 6−8 weeks, which were housed in designated specific pathogen-free (SPF) facilities. The Committee for Animal Care and Use of Laboratory Animals at Chengdu University of Traditional Chinese Medicine established guidelines for all animal research, which were followed (Approval No. 2021-143).

Autoimmune hepatitis in mice was induced by Con A following a previously established protocol with slight adjustments.[23] ROF was dissolved in 0.5% sodium carboxymethylcellulose, whereas Con A was given intravenously after being dissolved in pyrogen-free saline (PBS) at a dosage of 20 mg/kg. The modes and dosages of ROF administration in animal studies were set based on prior published research.[21] For the survival assessment, there were two groups in the study (n = 8 each group) as outlined: (i) Con A, and (ii) Con A + ROF-H (40 mg/kg). Mice in group i were orally administered the vehicle, while those in group ii were subjected to a 7-day oral pretreatment of ROF-H. Subsequently, each mouse received a tail-based injection of Con A, and the mortality rate was assessed after a complete 72 h period.

In the mechanism analysis experiment, the mice were randomly allocated into five groups, each consisting of six mice, as outlined below: (i) Normal, (ii) Con A, (iii) Con A + 20 mg/kg of ROF (ROF-L), (iv) Con A + 40 mg/kg of ROF (ROF-H), and (v) Con A + 200 mg/kg of BIF (positive drug). Mice in each group receiving either ROF-L, ROF-H, or BIF treatment were given their respective doses orally once daily for 7 days. In contrast, the groups i and ii were simultaneously administered the vehicle orally for 7 days. Then the mice in groups ii−v were injected with Con A, whereas the normal group received an equal amount of PBS. Eight hours after being exposed to Con A, the mice were euthanized to collect samples.

2.5. Serum Biochemical and Oxidative Stress-Related Indicators Analyses. The detection kits of aspartate aminotransferase (AST) (#140220009), alanine aminotransferase (ALT) (#140123001), alkaline phosphatase (ALP) (#140322002), and lactate dehydrogenase (LDH) (#142720008) were purchased from Mindray Bio-Medical Electronics Co., Ltd. (Shenzhen, China). In order to assess hepatic function, the ALT and AST levels, along with LDH and ALP concentrations in serum, were assessed by using the BS-240-VET automatic biochemistry analyzer (Mindray).

Furthermore, the malondialdehyde (MDA) assay kit (no. S0131S) was obtained from Beyotime (Shanghai, China). The detection kits of reduced glutathione (GSH) (#G0206W) and superoxide dismutase (SOD) (#G0101W) were both obtained from Grace Biotechnology Co.,Ltd. (Suzhou, China). Hepatic tissues were homogenized and dissolved in extraction buffer, and the GSH, SOD, and MDA expression levels were assayed

https://doi.org/10.1021/acsomega.4c07915
ACS Omega 2024, 9, 43233−43251

using the appropriate kits according to the instructions provided by the manufacturers.

2.6. Histological Examination. Following the sacrifice of the mice, hepatic tissue samples were obtained and preserved in 4% paraformaldehyde. Thereafter, the tissues were encased in paraffin, sliced into 5 μm thick sections, and kept at room temperature. The samples were dyed with H&E using standard methods and observed under a Pannoramic 250 Flash scanner (3DHISTECH, Hungary) at 100× or 400× magnification, with three fields per slide. The hepatic lesions were assessed based on the degree of necrosis and inflammation, with scoring ranging from 0 for no lesions to 4 for severe lesions. The detailed scoring criteria were as follows: 0, none; 1, very mild; 2, mild (≤30%); 3, moderate (≤60%); 4, severe (≥60%).[24]

2.7. Immunohistochemistry (IHC) and Immunofluorescence (IF) Analyses. Thin sections of hepatic tissues were treated to remove paraffin and restore hydration. They were then placed in a sodium citrate buffer with a pH of 6.0 for antigen retrieval and allowed to cool. Following this, endogenous peroxidase activity was suppressed for a duration of 10 min through the application of a 0.3% (v/v) hydrogen peroxide solution in methanol. After being incubated with a 10% goat serum blocking solution for 30 min, the samples were subjected to a series of antibodies overnight including CD4 (1:300), Ly-6G (1:200), cleaved-caspase-3 (1:400), Bax (1:200), p-JAK2 (1:200), p-STAT1 (1:400), and p-STAT3 (1:200). Following two rounds of washing, the samples underwent a 30 min incubation at room temperature with a secondary antibody diluted at a ratio of 1:100. The cell nuclei were subsequently stained with hematoxylin following the color development using the DAB kit (#DA1010, Solarbio). The Pannoramic Viewer was utilized for viewing and capturing the images at 400× magnification with three fields per slide. The integrated optical density (IOD), or the quantity of positive cells in the IHC staining, was quantified by utilizing the ImageJ 6.0 software program within each lesion.

In order to assess the Th cell expression levels in the spleens, CD4 antibodies were used to stain the cut sections at 4 °C for a whole night. Following three washes, the slides underwent staining with Alexa Fluor 488-labeled goat anti-rabbit IgG(H+L) (no. A0423, Beyotime Biotechnology) for 1 h at room temperature. Then, the slides were dyed with DAPI after another round of washing. Observation and photography of the slides were conducted by using a fluorescence microscope, and the fluorescence intensities of CD4 were quantified by using ImageJ software.

2.8. Flow Cytometric Analysis for $CD4^+$ IFN-γ^+ and $CD4^+$ IL-17^+ T Cells in Hepatic Mononuclear Cells (MNCs). The MNCs were obtained using the method previously outlined.[25] In short, the liver of each mouse was first flushed with PBS to remove blood until the liver became pale. Subsequently, the harvested tissues were adequately ground and passed using a cell strainer (200 μm). The resultant cell suspensions were gathered and reconstituted in 40% Percoll and carefully layered over 70% Percoll. After that, the mixture was subjected to centrifugation at 2200 rpm for 20 min. After being separated from the interphase, hepatic MNCs were treated for 5 min with red blood cell lysis buffer. Then the cells were rinsed with RPMI 1640 medium and gathered. To quantify the levels of IFN-γ^+ and IL-17^+ in $CD4^+$ T cells derived from hepatic MNCs, a leukocyte activation cocktail containing BD GolgiPlug was added to the MNCs and subsequently then kept for 4−6 h at 37 °C in a humidified CO_2 incubator. The MNCs were then treated with the antibodies of CD3 and CD4 at 4 °C for 30 min before being fixed and permeabilized with the fixation/permeablization kit. Ultimately, the cells underwent flow cytometry analysis after being tagged for 30 min at 4 °C with either an antimouse IFN-γ or IL-17 antibody.

2.9. Cell Isolation and Culture. Negative magnetic sorting was used to separate $CD4^+$ T cells from the spleens of naive C57BL/6J mice using the Dynabeads Untouched Mouse CD4 cells kit (Thermo Scientific, USA). The cellular purity was assessed through flow cytometry utilizing antimouse CD3 and CD4 antibodies and was routinely greater than 90%. The purified $CD4^+$ T cells were cultivated in RPMI-1640 medium (#10491, Solarbio) with the addition of 10% fetal bovine serum (FBS), 1% penicillin−streptomycin solution, and 50 μM β-mercaptoethanol in a 37 °C humidified CO_2 (5%) incubator.

A two-step perfusion method was employed to isolate primary hepatocytes.[26] Mice were euthanized and subjected to a 75% ethanol bath before undergoing laparotomy. Subsequently, 10 mL of preheated D-Hanks' buffer was perfused into the hepatic portal vein for 10 min, followed by the addition of 5 mL of type II collagenase solution (0.8 mg/mL; MCE, #9001-12-1). Hepatic tissue fragments were then incubated for 30 min in a shaking water bath with a collagenase II solution. Then, the primary hepatocytes were centrifuged for 5 min and supplemented with RPMI-1640 culture media. After cell viability detected by Trypan blue exclusion, the cells were grown in an incubator with humidified CO_2 (5%) at 37 °C using RPMI-1640 medium supplemented with 10% FBS and 1% penicillin−streptomycin solution.

2.10. Cell Viability Assay. $CD4^+$ T cells and primary hepatocytes were incubated with ROF concentrations ranging from 5 to 20 μM with or without Con A (5 or 10 μg/mL) stimulation for 24 h. Then, to each well was added 10 μL of CCK-8 solution (#AR1160, Boster), and the samples were incubated for a further 2−3 h. The absorbance values of the samples were subsequently gauged at 450 nm using SpectraMax Id5 (Molecular Devices).

2.11. T-Cell Differentiation. The T-cell differentiation experiment was carried out according to earlier reports.[27] Briefly, immature anti-CD3 (2 μg/mL, #BE0002, BioXcell) coated plates and soluble anti-CD28 (2 μg/mL, #BE0328, BioXcell) were used to incubate the purified $CD4^+$ T cells. Cells were then treated with anti-IL-4 antibody (10 μg/mL, #504102, BioLegend), IL-12 recombinant protein (10 ng/mL, #210-12, PEPROTECH), and IL-2 recombinant protein (2 IU, #212-12, PEPROTECH) to stimulate Th 1 cells differentiation. Furthermore, the cells were also treated with anti-IFN-γ (10 μg/mL, #505801, BioLegend), anti-IL-4 (10 μg/mL), TGF-β1 recombinant protein (3 ng/mL, #763102, BioLegend), IL-6 recombinant protein (30 ng/mL, #216-16, PEPROTECH), and 10 ng/mL IL-1β (#211-11B, PEPROTECH) to stimulate Th17 cells differentiation. At the onset of culture, ROF (20 μM) or TOF (1 μM) was added. After 3 days of treatment, differentiated cells were harvested to isolate total RNA to assess the expression of specific transcription factors *T-bet* or *RORγt*.

2.12. Enzyme-Linked Immunosorbent Assay (ELISA). Mouse enzyme-linked immunosorbent assay (ELISA) kits for TNF-α (E-EL-M3063), IFN-γ (E-EL-M0048), IL-2 (E-EL-M0042), and IL-17 (E-EL-M0047) were acquired from Elabscience (Wuhan, China). The cytokine levels of TNF-α,

https://doi.org/10.1021/acsomega.4c07915
ACS Omega 2024, 9, 43233−43251

IFN-γ, and IL-2 in serum were measured in accordance with the guidelines provided by the manufacturer. For *in vitro* experiments, $CD4^+$ T cells were grown under circumstances that promote Th1 and Th17 polarization. The IFN-γ and IL-17 concentrations in cellular supernatants were examined by using relevant ELISA kits.

2.13. AnnexinV/Propidium Iodide (PI) Apoptosis Assay. Primary hepatocytes were incubated with or without ROF (20 μM) for 6 h and then stimulated with Con A (10 μg/mL) for 24 h. The cells were then washed, resuspended, and stained with FITC and PI for approximately 15 min. The quantification of stained apoptotic cells was performed by utilizing flow cytometry (FACSCalibur; BD Biosciences, Franklin Lakes, NJ, USA).

2.14. Determination of mRNA via Reverse-Transcriptase Polymerase Chain Reaction (RT-PCR). The frozen hepatic tissues or harvested $CD4^+$ T cells were employed to get total RNA with RNA isolation kits obtained from FOREGENE (Chengdu, China). Next, a FastKing gDNA Dispelling RT SuperMix (TIANGEN, Beijing, China) was used to transform the RNA into cDNA. Real time PCR Easy-SYBR Green I (FOREGENE) was utilized for PCR amplification in a reaction system with 20 μL. The PCR conditions were carried out in the following manner: first denaturation for 3 min at 95 °C, then annealing for 10 s at 65 °C, extending to 20 s at 72 °C, and so on for a total of 40 cycles. The mRNA levels of interest were standardized against the reference gene GAPDH and translated into fold changes using the following formula: fold change = $2^{-\Delta\Delta CT}$, where ΔΔCT is equal to (CT Target-CT GAPDH). The primer sequences utilized for the investigation were documented in Table 1.

Table 1. Primers employed in this investigation

gene	name	sequence (5′ to 3′)
GAPDH	*GAPDH*-F	CAGTGGCAAAGTGGAGATTGTTG
	GAPDH-R	TCGCTCCTGGAAGATGGTGAT
TNF-α	*TNF-α*-F	ACGGCATGGATCTCAAAGACA
	TNF-α-R	GTGAGGAGCACGTAGTCGG
IL-6	*IL-6*-F	GTATGAACAACGATGATGCAC
	IL-6-R	CTCCAGAAGACCAGAGGAAA
IFN-γ	*IFN-γ*-F	TGAGGTCAACAACCCACA
	IFN-γ-R	ACTCCTTTTCCGCTTCCT
IL-17	*IL-17*-F	TTCACTTTCAGGGTCGAGA
	IL-17-R	GGGGTTTCTTAGGGGTCA
IL-2	*IL-2*-F	TAAAGGGCTCTGACAACACA
	IL-2-R	GAAAGTCCACCACAGTTGCT
T-bet	*T-bet*-F	AGCAAGGACGGCGAATGTT
	T-bet-R	GGGTGGACATATAAGCGGTTC
RORγt	*RORγt*-F	GACCCACACCTCACAAATTGA
	RORγt-R	AGTAGGCCACATTACACTGCT

2.15. Western Blotting. The frozen hepatic tissues, collected $CD4^+$ T cells, and primary hepatocytes were subjected to lysis on ice using a radioimmunoprecipitation assay (RIPA) lysis solution (no. AR0102, BOSTER) containing phosphatase and protease inhibitors (no. AR1195 and #AR1182, BOSTER) for a duration of 30 min. Following 20 min at 4 °C and 12 000 rpm centrifugation of the lysates, the BCA protein assay kit (#AR1189, BOSTER) was utilized to test and adjust the lysate concentrations. The Tris-glycine gel containing approximately 40 μg of total proteins was used for sodium dodecyl sulfate−polyacrylamide gel electrophoresis (SDS-PAGE) separation at a concentration of 10% or 12%. After transferring the proteins, the polyvinylidene difluoride (PVDF) membranes were using 5% skim milk to block for 1 h. After that, the membranes were incubated overnight at 4 °C with the selected primary antibodies. The antibodies for cleaved-caspase-3, cleaved-caspase-9, Bax, Bcl-2, JAK2, p-JAK2, JAK3, p-JAK3, IL-6, STAT1, p-STAT1, STAT3, p-STAT3, and BNIP3 were diluted at a ratio of 1:1000, and β-actin (#BA2305, BOSTER) was diluted at a ratio of 1:5000 in the primary antibody dilution buffer. Following rinsing, the membranes were incubated for 1 h with HRP-conjugated AffiniPure goat anti-rabbit IgG (H+L) (#BA1055, BOSTER). A chemiluminescence reagent was used to identify the protein bands via the ChemiDoc XRS+ image analysis system, and ImageJ software was used to analyze the data.

2.16. Statistical Analyses. Based on the results of *in vitro* or *in vivo* investigations, the data were displayed as mean ± SEM in bar graphs, generated using GraphPad Prism version 10.1.2. Statistical analyses were conducted with an IBM SPSS 26.0. Significant variations were statistically compared through the utilization of one-way analysis of variance (ANOVA) in conjunction with Dunnett's post hoc test. For the non-parametric test, the Kruskal−Wallis one-way ANOVA test was employed when the data did not follow a normal distribution and exhibited unequal variances. For the statistical analysis of the differences in survival curves, the Kaplan−Meier method was conducted. A difference that was deemed statistically significant was defined as $P < 0.05$.

3. RESULTS

3.1. Bioinformatics Analysis of the Potential Mechanisms of ROF against AIH. Through database searches, a total of 301 targets for ROF and 1668 targets for AIH were identified with 119 targets found to overlap between the two (Figure 1B). The analysis of the PPI network revealed the presence of 114 nodes and 619 edges within the network, and the colored nodes represented the target proteins and the edges symbolize their interactions (Figure 1C). Using the Centiscape 2.2 plug-in, the top 54 genes, including TNF, ALB, AKT1, TP53, CASP3, EGFR, IL-2, JAK2, and JAK3, were identified and classified as hub genes (Figure 1C). The KEGG enrichment heatmap revealed potential involvement of ROF in critical pathways such as Pathways in cancer, Lipid and atherosclerosis, Proteoglycans in cancer, and Th17 cell differentiation (Figure 1D). Further GO enrichment analyses of MCODE networks highlighted the regulatory potential of the ROF in immune functions (Figure 1E). For example, MCODE1 exhibited significant associations with biological processes such as Pathways in cancer ($\log_{10} p = -14.2$), PI3K-AKT signaling pathway ($\log_{10} p = -13.7$), and Th1 and Th2 cell differentiation ($\log_{10} p = -11.5$). Similarly, MCODE2 was correlated with Proteoglycans in cancer ($\log_{10} p = -14.8$), Rap1 signaling pathway ($\log_{10} p = -14.6$), and Ras signaling pathway ($\log_{10} p = -14.2$), while MCODE3 was linked to the IL-17 signaling pathway ($\log_{10} p = -7.5$), prostate cancer ($\log_{10} p = -7.5$), and the TNF signaling pathway ($\log_{10} p = -7.2$). In summary, the bioinformatics analysis suggested that ROF may possess the ability to alleviate AIH via modulation of T-cell-mediated adaptive immune responses and regulation of the apoptosis cascade.

3.2. Molecular Docking and Dynamic Simulation. As outlined in the core targets and the MCODE1 algorithm, JAK2

https://doi.org/10.1021/acsomega.4c07915
ACS Omega 2024, 9, 43233−43251

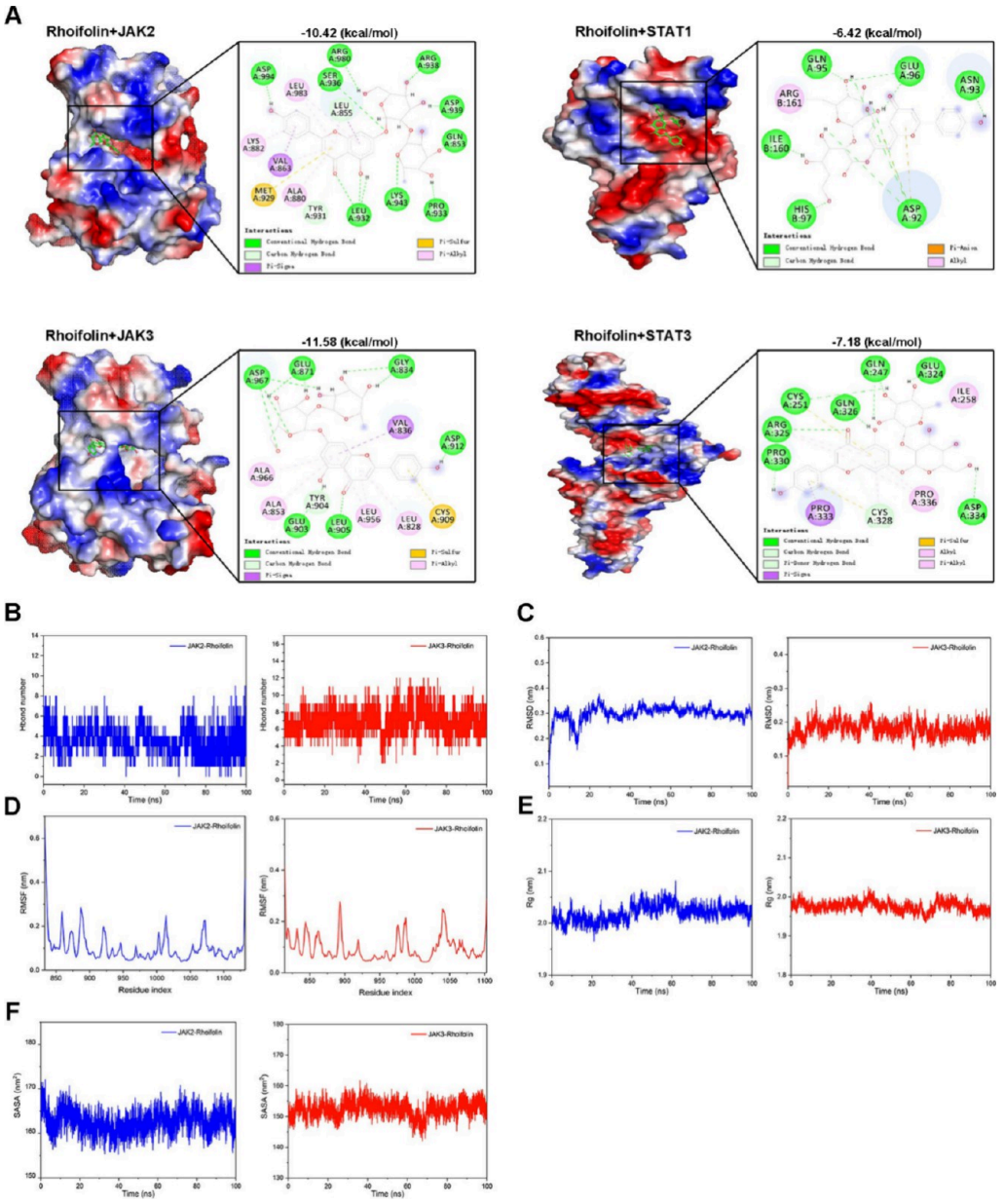

Figure 2. Molecular docking and dynamic simulations of ROF and JAKs/STATs signaling molecules (A) The binding modes of ROF toward JAK2, JAK3, STAT1, and STAT3. (B–F) The dynamic simulations of JAK2-ROF and JAK3-ROF complexes. The HBond (B), RMSD curves (C), RMSF values (D), Rg values (E), and SASA (F) were analyzed by GROMACS.

and JAK3 have been identified as significant hub genes for ROF in improving AIH. Simultaneously, the JAKs-regulated STATs signaling pathways play a vital part in T cell differentiation and the pathogenesis of AIH. Subsequently, molecular docking techniques were utilized to assess ROF's propensity for binding to these potential targets (Figure 2A). It is widely recognized that a binding energy of less than −4.25 kcal/mol suggests that the ligand molecule has the potential to bind to the receptor target to a certain degree. Furthermore, binding energies below −5.0 kcal/mol and −7.0 kcal/mol are indicative of good and strong binding affinities, respectively.[28] Our findings indicated that ROF exhibited favorable docking affinity with the protein molecules JAK2, JAK3, STAT1, and STAT3, resulting in binding energy scores of −10.42 (kcal/mol), −11.58 (kcal/mol), −6.42 (kcal/mol), and −7.18 (kcal/mol), respectively. Taking the docking of ROF and JAK2 as an example, it can form hydrogen bond interactions with the amino acids ASP-994, ARG-980, SER-936, ARG-938, ASP-939, GLN-853, LYS-943, PRO-933, and LEU-932 at the active site of the JAK2 protein, which is significant for anchoring ligand molecules in the protein's active pocket. Additionally, this compound can also form good hydrophobic interactions with LEU-983, LYS-882, VAL-863, MET-929, and ALA-880, which contributes importantly to the stability of small molecules. These results suggested that the ROF revealed robust and spontaneous interactions with the key proteins involved in the JAKs/STATs signaling pathways.

Additionally, molecular dynamic simulations were conducted to assess the stability of the binding interactions between ROF and JAKs. The hydrogen bond analysis revealed that an increased number of hydrogen bonds were established between JAK2/3 and ROF throughout the simulation, which

https://doi.org/10.1021/acsomega.4c07915
ACS Omega 2024, 9, 43233−43251

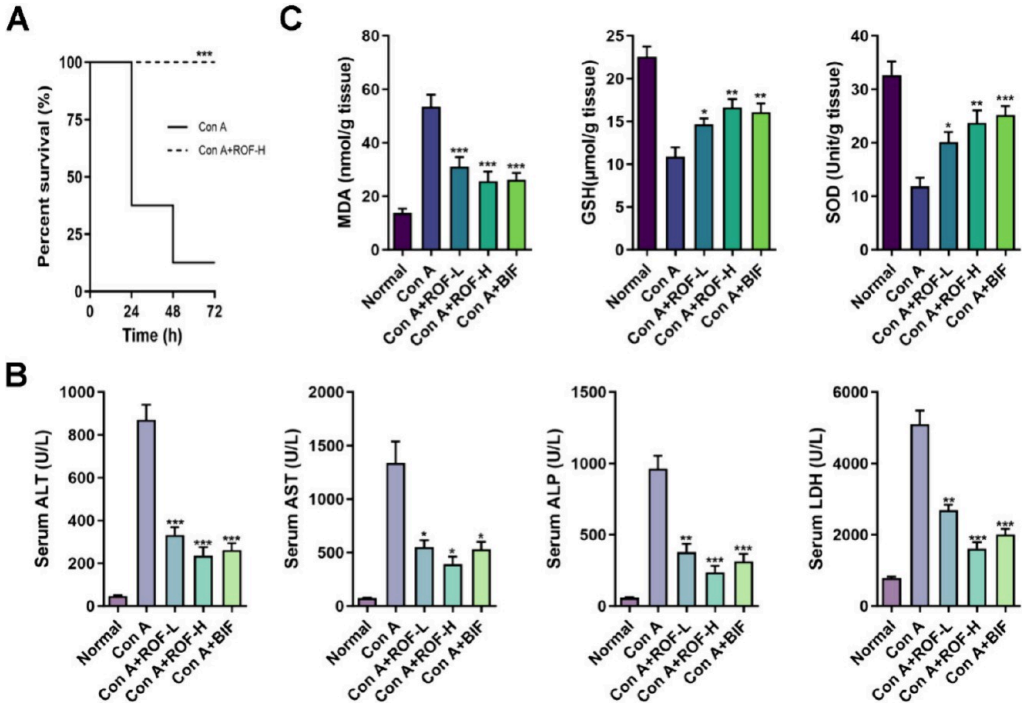

Figure 3. Effects of ROF on survival rate, biochemical indices, and oxidative stress in Con A-induced hepatitis (A) The influence of ROF on mortality caused by Con A for up to 72 h (n = 8). (B) The serum concentrations of ALT, AST, ALP, and LDH were monitored following the Con A-injection in mice (n = 6). (C) The MDA, GSH, and SOD levels were assessed in hepatic tissues (n = 6). The values are presented as the mean ± SEM. *P < 0.05, **P < 0.01, ***P < 0.001 vs the Con A group.

aligns with the findings from molecular docking studies (Figure 2B). Root mean square deviation (RMSD) quantifies the sum of deviations of all atomic positions at a specific moment from the initial conformation. Monitoring the RMSD of a protein can provide valuable insights into the structural conformation of the complex throughout the simulation process, assess the stability of the system, and evaluate the flexibility of the molecule.[29] The RMSD curves indicated that the ROF-JAK2 or ROF-JAK3 complex has average RMSD values of less than 3.5 or 2.0 Å, respectively, entering dynamic equilibrium around 20 and 10 ns (Figure 2C). This suggested that after dynamic adjustments, ROF could still form stable complexes with JAK2/3 effectively. The root mean square fluctuation (RMSF) values for the JAK2-ROF and JAK3-ROF complexes uncovered that only a small number of amino acids exhibited significant conformational changes, particularly near residues 890 and 1040 (Figure 2D). The primary reason for this was that these amino acids were located in the hinge region of the protein, which possessed a high degree of flexibility, rendering their conformations susceptible to alterations during the simulation process. However, the conformational changes of the majority of amino acids remained within an acceptable range. Additionally, the radius of gyration (R_g) values for the JAK2-ROF and JAK3-ROF complexes were stable at about 2.0 nm, revealing that the binding of small molecules to proteins was relatively compact (Figure 2E). Furthermore, the solvent accessible surface area (SASA) offers a visual representation of the accessibility of a protein's surface, illustrating the degree to which the protein surface is exposed to the surrounding solvent.[29] As shown in Figure 2F, over the course of 100 ns, the SASA of the JAK2-ROF complex exhibited a notable reduction, suggesting that the overall stability of the complex improved following kinetic modifications. In contrast, the SASA of the JAK3-ROF complex showed fluctuations without a decline, essentially maintaining its original level. This may indicate that the complex itself has good stability and that no significant conformational changes occurred. Finally, the g_MMPBSA method was employed to calculate the G binding energy of ROF with JAK2 and JAK3 proteins. The results indicated that the G binding energy of ROF with the JAK2 protein was −102.23 ± 12.565 kJ/mol, while the G binding energy with the JAK3 protein was −164.376 ± 14.505 kJ/mol. In summary, ROF exhibited a strong affinity for the JAK2 and JAK3 proteins. This affinity can facilitate the formation of stable complexes between small molecules and proteins, thereby exerting significant biological effects.

3.3. ROF Improved the Survival Rate and Reduced Con A-Induced Blood Biochemical and Oxidative Stress-Related Indexes. To investigate the possible protective effects of ROF in mitigating hepatic damage-induced mortality in mice triggered by Con A, we initially performed a survival evaluation of the animals for a period of 72 h after administration of the conventionally lethal dosage of Con A (20 mg/kg). The results revealed that mice pretreated with ROF-H demonstrated a notably higher survival rate (up to 100%) in contrast to the mice in the group of the Con A model (Figure 3A).

Numerous studies have indicated the optimal timing for conducting tests on relevant hepatic protection mechanisms to be 8−12 h after the induction of Con A stimulation.[30] Consequently, we proceeded with the collection of samples and the subsequent analysis 8 h after Con A injection. As illustrated in Figure 3B, the administration of Con A led to significantly increased serum levels of liver damage biomarkers, including AST, ALT, LDH, and ALP, when compared to the control group. Nevertheless, the increase in elevation was

https://doi.org/10.1021/acsomega.4c07915
ACS Omega 2024, 9, 43233−43251

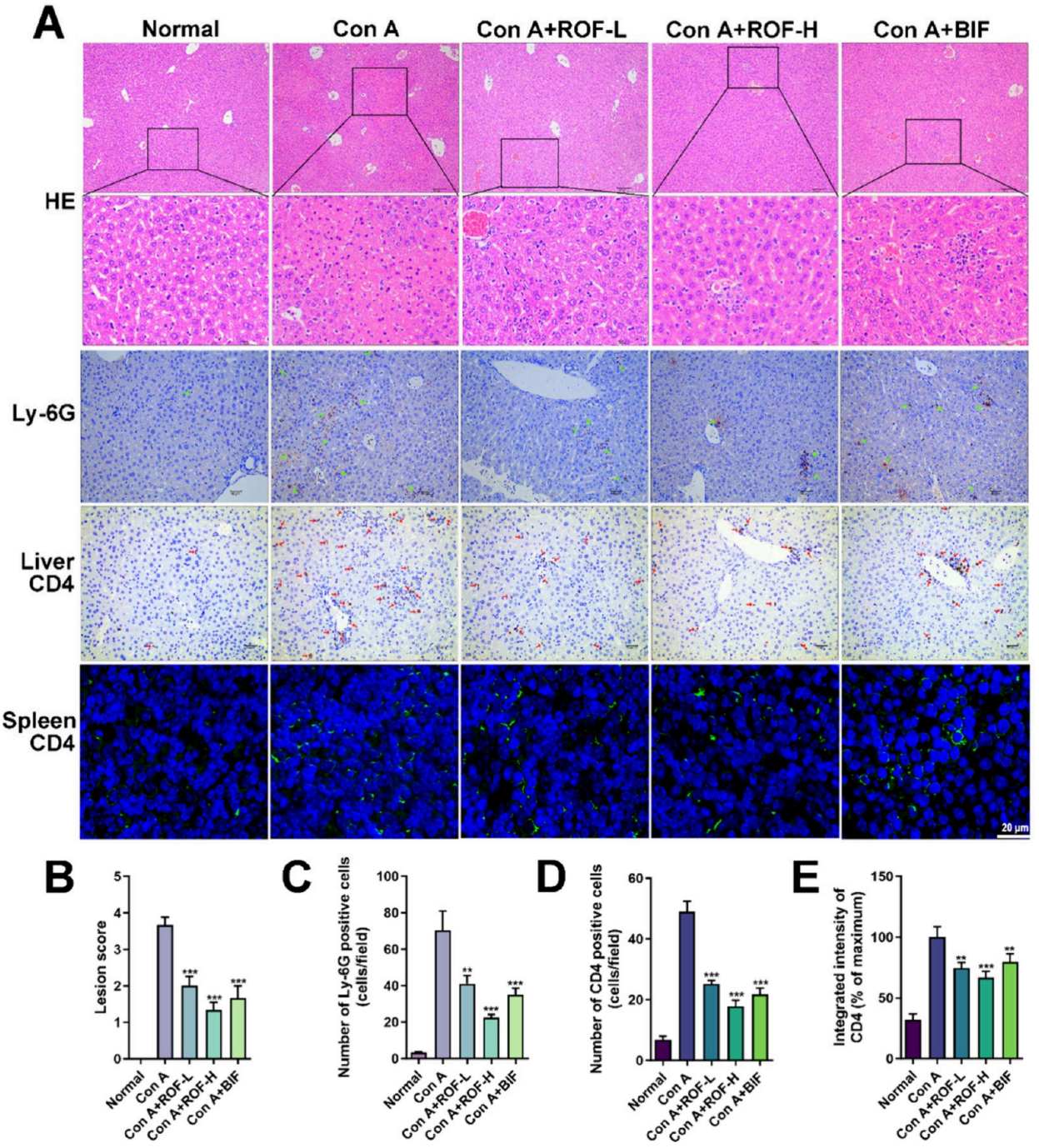

Figure 4. Effects of ROF on hepatic injury and immune cells infiltration (A) H&E staining (scale bar = 100 or 10 μm) for hepatic lesions, IHC analysis of Ly-6G and CD4 cells in hepatic tissues (scale bar = 40 μm), and IF staining for CD4 in spleens (scale bar = 20 μm) (n = 3). (B) The lesion score was calculated. (C, D) The positive cell numbers of Ly-6G and CD4 were randomly counted by ImageJ. (E) Integrated intensity of CD4 in spleen tissues. The values are presented as mean ± SEM. $^{**}P < 0.01$, $^{***}P < 0.001$ vs the Con A group.

notably reduced in animals that received pretreatment with ROF-L or ROF-H, as compared to the Con A group.

There is an increasing body of evidence indicating that oxidative stress is significantly involved in the hepatocyte apoptosis and hepatic damage caused by Con A.[31] We next assessed the concentrations of oxidative stress biomarkers, including MDA, GSH, and SOD, in hepatic tissues (Figure 3C). The findings demonstrated that the injection of Con A raised the amount of MDA content in the hepatic tissues while decreasing the SOD and GSH activity. However, the ROF pretreatment effectively improved the oxidative stress by reducing lipid peroxidation products and enhancing antioxidant levels as compared to the Con A group.

3.4. ROF Improved Con A-Induced Hepatic Injury and Inhibited Immune Cells Infiltration. As depicted in Figure 4A, the histopathological results were in line with the biochemical results. The samples from the control group animals exhibited typical hepatic tissue without evidence of lesions, whereas hepatic tissues in the Con A group showed signs of hepatic damage, including apoptosis, necrosis, and inflammatory infiltration. Moreover, the hepatic lesion score was notably higher in contrast to the Normal group (Figure

https://doi.org/10.1021/acsomega.4c07915
ACS Omega 2024, 9, 43233−43251

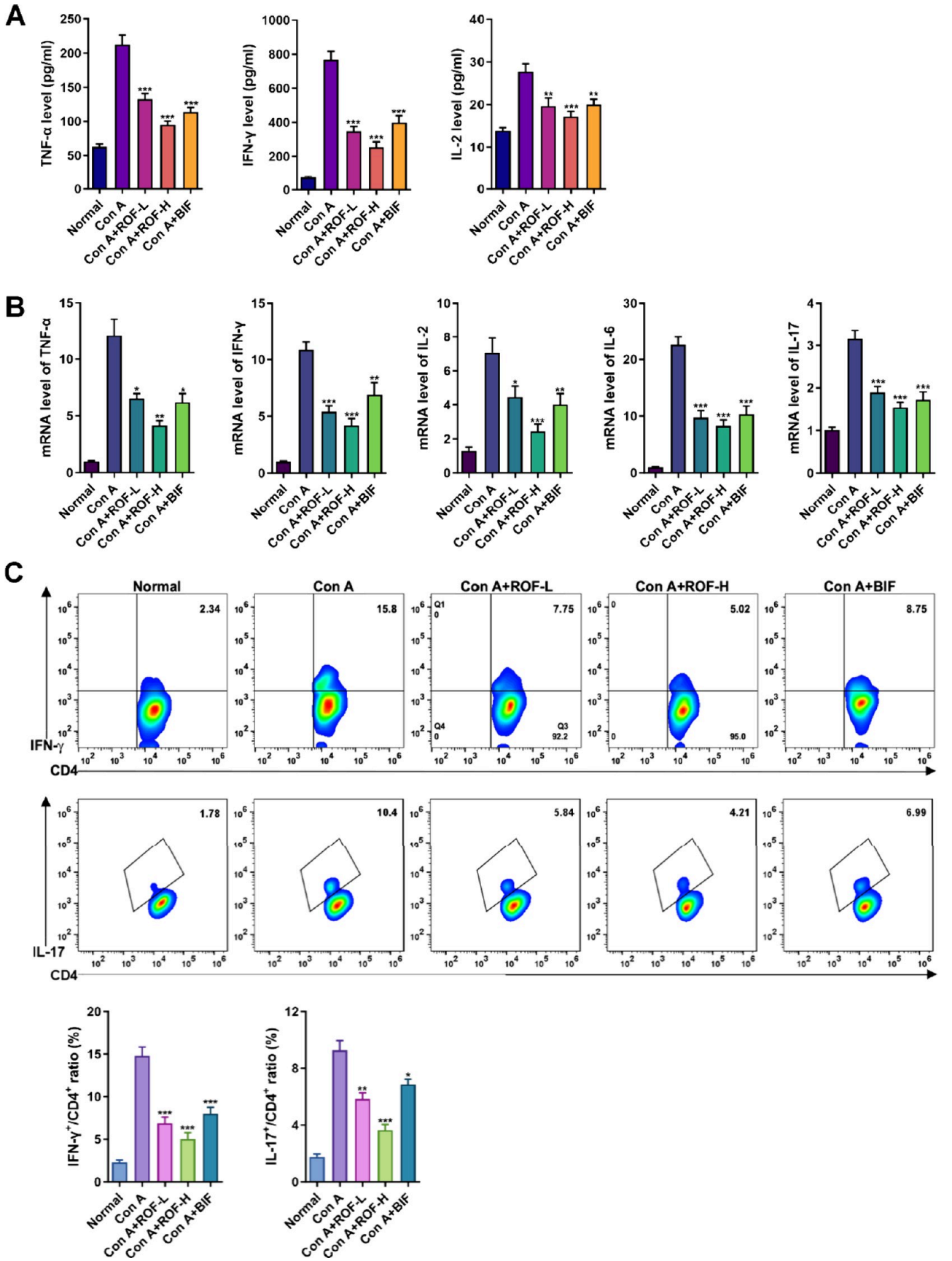

Figure 5. Effects of ROF on inflammatory cytokines and hepatic $CD4^+$ T cells (A) The concentrations of TNF-α, IFN-γ, and IL-2 in serum were measured using ELISA (n = 6). (B) The mRNA levels of *TNF-α*, *IFN-γ*, *IL-2*, *IL-6*, and *IL-17* in hepatic tissues were determined using RT-PCR (n = 6). (C) Analysis of $CD4^+$ IFN-γ^+ and $CD4^+$ IL-17^+ T cells in hepatic tissues by flow cytometry (n = 3). The data for each group are presented as the mean ± SEM. *P < 0.05, **P < 0.01, ***P < 0.001 vs the Con A group.

https://doi.org/10.1021/acsomega.4c07915
ACS Omega 2024, 9, 43233−43251

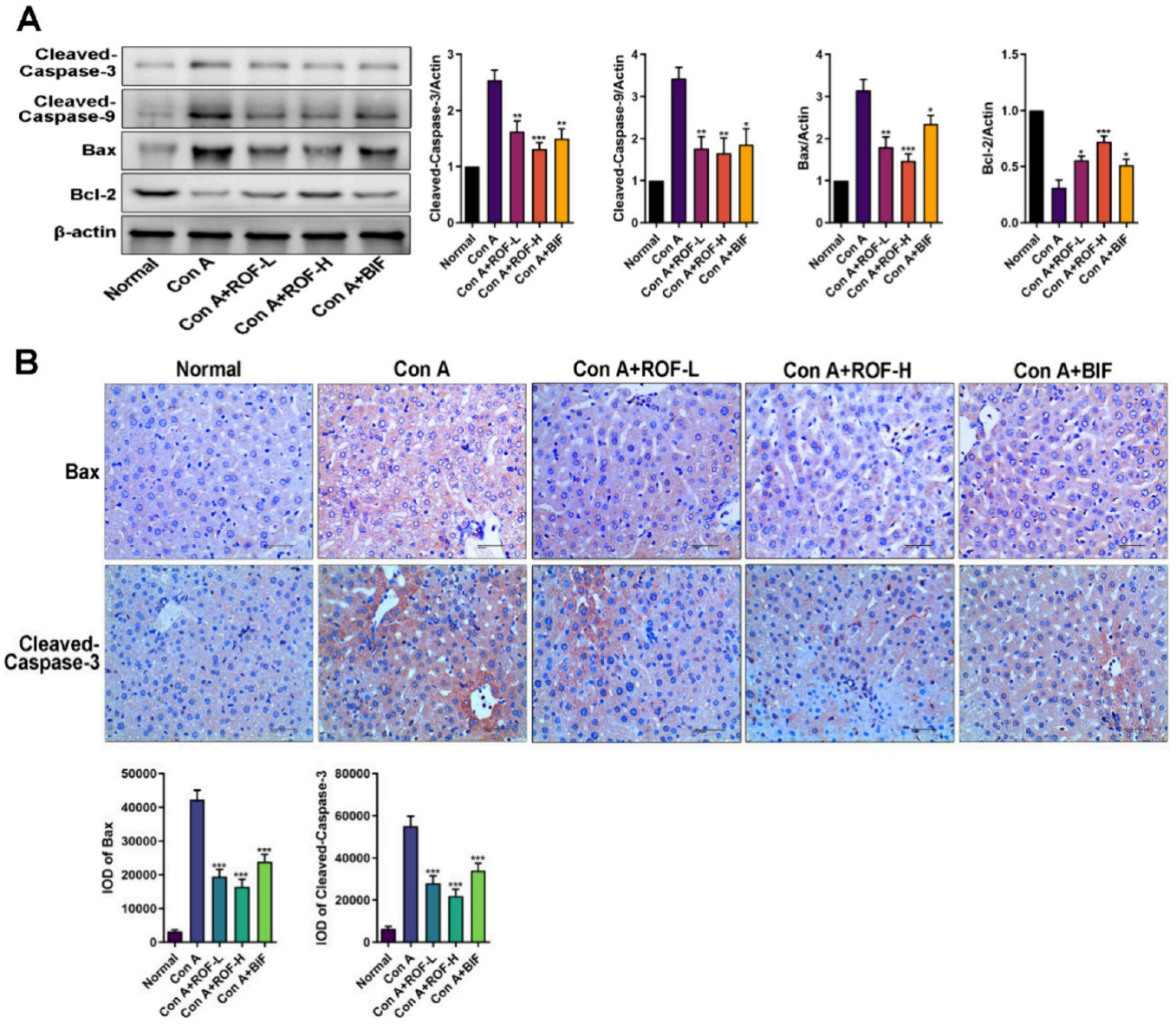

Figure 6. Effects of ROF on apoptosis in Con A-induced hepatitis (A) Western blotting of Cleaved-Caspase-3, Cleaved-Caspase-9, Bcl-2, and Bax (n = 3). The grayscale values of the target bands were standardized against β-actin. (B) IHC staining of Bax and Cleaved-Caspase-3 (n = 3; scale bar = 40 μm), and the IODs of these proteins were detected using ImageJ. Results are represented as mean ± SEM. *P < 0.05, **P < 0.01, ***P < 0.001 vs the Con A group.

4B). However, The ROF pretreatment effectively inhibited the progression of Con A-induced lesions and significantly ameliorated the aforementioned pathological indicators. To confirm the potential of ROF to limit the infiltration of immune cells, the presence of Ly-6G and CD4 positive cells in the liver or spleen was examined using immunohistochemistry or immunofluorescence (Figure 4A,C−E). The samples from the Con A group exhibited a notable rise in Ly-6G- and CD4-positive cells compared with the normal group. Similarly, in the spleen tissue of the Con A group, the fluorescence intensity of CD4 cells was significantly greater than that observed in the normal group. Conversely, ROF pretreatments effectively mitigated the Con A-induced increase in neutrophils and $CD4^+$ T cells infiltration either in liver or spleen.

3.5. ROF Attenuated Inflammatory Cytokine Levels and Subtypes of $CD4^+$ T Cells Induced by Con A Administration. Numerous reports have confirmed that TNF-α, IFN-γ, IL-2, and IL-17 facilitate hepatic injury, while IL-6 exhibits variable consequences according on the stage of Con A-induced AIH.[32] To determine whether ROF could affect cytokine levels, we used ELISA kits or PCR to measure the expression of IFN-γ, TNF-α, IL-2, IL-6, and IL-17 in serum or hepatic tissues (Figure 5A,B). The results demonstrated that serum cytokines TNF-α and IFN-γ were significantly upregulated in the Con A challenge group, whereas IL-2 levels were marginally increased in comparison to the normal group. Nevertheless, the cytokine production caused by Con A was lessened by ROF, as evidenced by the significantly lower levels of IFN-γ, TNF-α, and IL-2 in the circulation of the mice treated with ROF. Moreover, there were also significant differences in the gene expression levels including *TNF-α*, *IFN-γ*, *IL-2*, *IL-6*, and *IL-17* among the groups in hepatic tissues.

Additionally, the percentage of infiltrating Th1 and Th17 cells in Con A-induced AIH mice with or without ROF

https://doi.org/10.1021/acsomega.4c07915
ACS Omega 2024, 9, 43233−43251

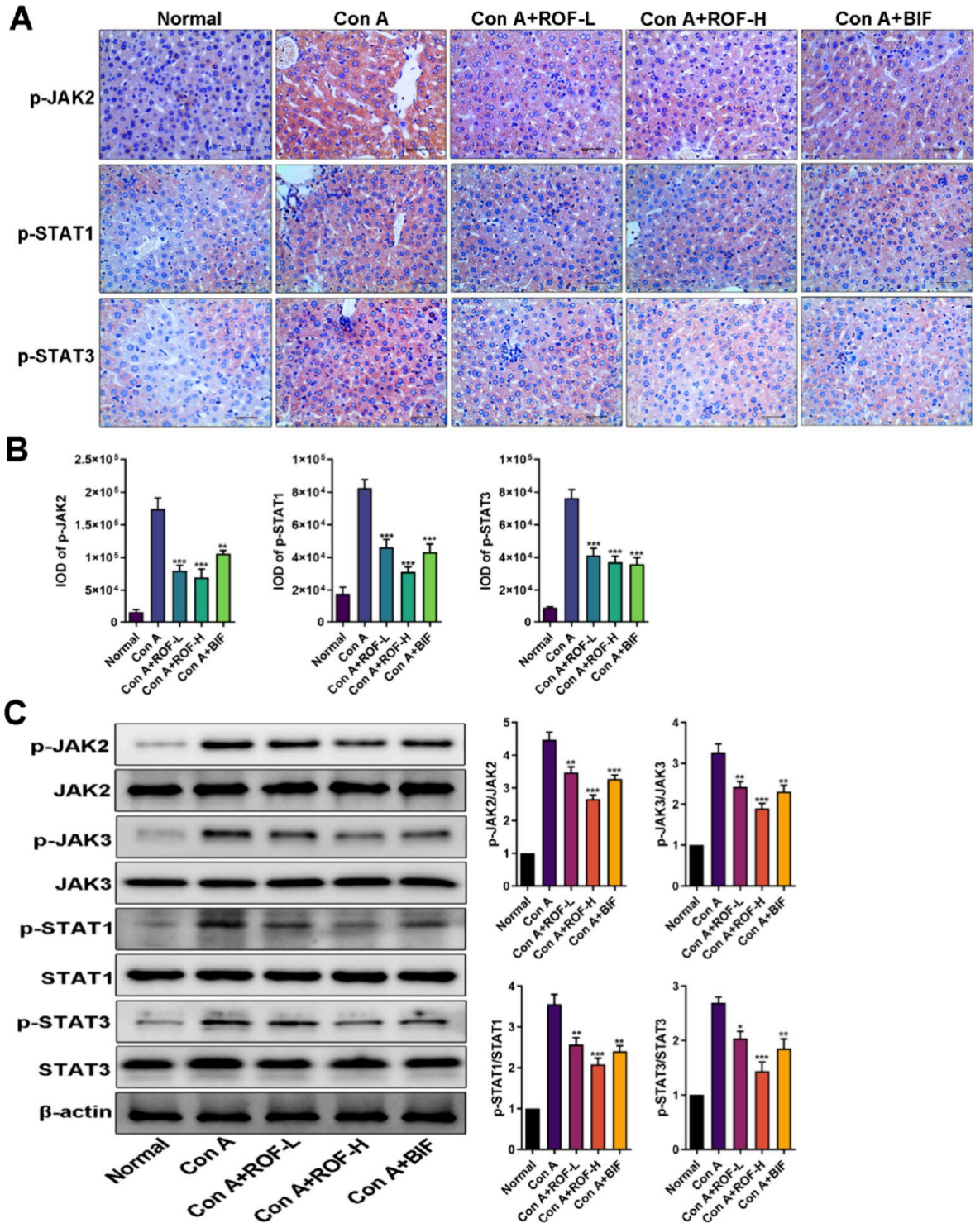

Figure 7. Effects of ROF on the JAK2/3-STAT1/3 signaling pathways in Con A-induced hepatitis (A) The phosphorylated levels of JAK2, STAT1, and STAT3 were measured in hepatic tissues using IHC staining (n = 3; scale bar = 40 μm). (B) The IODs of each protein were detected by using ImageJ. (C) The JAK2/3-STAT1/3 signaling molecules were measured in hepatic tissues with Western blot analysis (n = 3). The gray value analysis was standardized using the intensity of β-actin and is depicted in bar graphs. The results are presented as mean ± SEM. *P < 0.05, **P < 0.01, ***P < 0.001 vs the Con A group.

treatment was evaluated to examine whether ROF could modulate the $CD4^+$ T cell response during hepatic damage (Figure 5C). The findings revealed that Con A injection resulted in a considerable infiltration of Th1 and Th17 cells in the livers. However, in Con A-induced mice models, ROF administration resulted in significantly lower infiltration of Th1 and Th17 lineages in contrast to those receiving saline as a control, especially those receiving a high ROF dosage.

3.6. ROF Downregulated Hepatocyte Apoptosis in Con A-Induced Hepatitis. The apoptosis process in hepatocytes is an important component of the onset of drug-induced hepatic damage. Con A has the ability to trigger

https://doi.org/10.1021/acsomega.4c07915
ACS Omega 2024, 9, 43233−43251

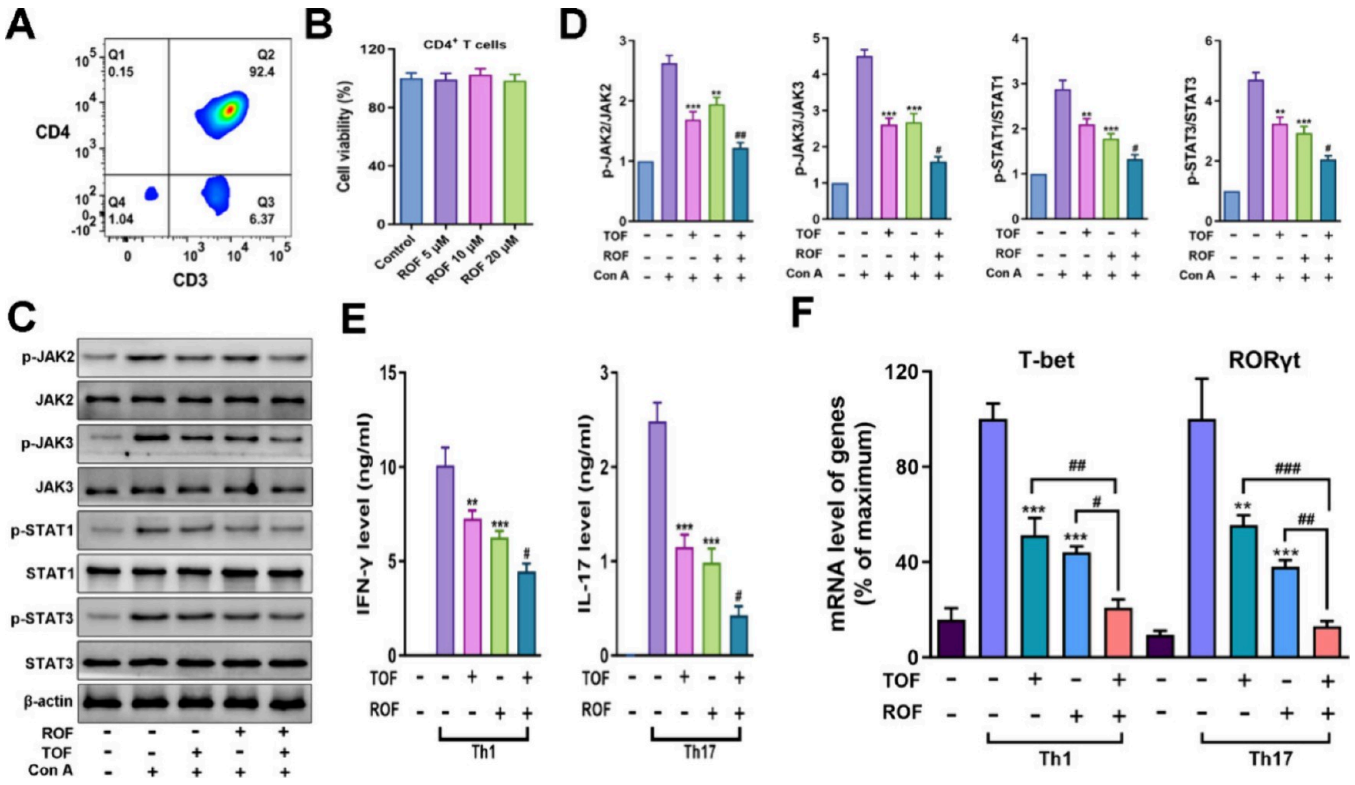

Figure 8. Effects of ROF on Th1/Th17 cells differentiation *in vitro* (A) The purity of isolated $CD4^+$ T cells was measured by flow cytometry. (B) The viability of $CD4^+$ T cells following 5−20 μM ROF treatments for 24 h was assessed utilizing the CCK-8 assay. (C, D) $CD4^+$ T cells were pre-exposed for 1 h to ROF (20 μM), TOF (1 μM), or ROF (20 μM) + TOF (1 μM), followed by stimulation with Con A for 24 h. The levels of p-JAK2, p-JAK3, p-STAT1, and p-STAT3 were monitored by Western blotting and normalized to each protein's total concentration in the graphs. (E) The generation of IFN-γ or IL-17 in the cellular supernatants of Th1 or Th17 subtypes were measured using ELISA. (F) The gene expression levels of *T-bet* or *RORγt* in differentiated T cells were evaluated by PCR. The values are presented as mean ± SEM (n = 3). $^{**}P < 0.01$, $^{***}P < 0.001$ vs the Con A group. $^{\#}P < 0.05$, $^{\#\#}P < 0.01$, $^{\#\#\#}P < 0.001$ vs the ROF only group or TOF only group.

apoptosis in hepatocytes through various pathways, consequently leading to damage in the liver.[16] In our study, the protein Bcl-2, recognized for its antiapoptotic properties, was assessed as well as the proapoptotic proteins such as cleaved-caspase-3, cleaved-caspase-9, and Bax by the utilization of Western blot analysis. The findings indicated a notable increase in the expression levels of pro-apoptotic proteins in the Con A model group as compared to the normal group. However, the ROF administration obviously decreased these proapoptotic proteins' expression in the hepatic tissues (Figure 6A). Additionally, there was a notable decline in Bcl-2 expression in the Con A model group, while the ROF pretreatment groups showed an increase in its expression (Figure 6A). In line with these results, the immunohistochemical examination of Bax and cleaved-caspase-3 in mouse livers also revealed a marked change in apoptosis in the groups that received ROF treatment in contrast to the Con A group (Figure 6B).

3.7. ROF Pretreatment Alleviated the JAK2/3-STAT1/3 Signaling Pathways after Con A Challenge. To further study the effects of ROF on the regulation of JAKs/STATs signaling pathways *in vivo*, we measured the expression levels of relevant phosphorylated proteins in hepatic tissues. As demonstrated in Figure 7A,B, when comparing the Con A model group to the normal group, IHC analysis revealed a significant elevation of JAK2, STAT1, STAT3 phosphorylated protein expression levels. However, pretreatment with ROF restored the impact caused by Con A. Furthermore, our Western blotting results also showed that the production of JAK2/3/-STAT1/3 signaling phosphorylated molecules was significantly increased after the Con A treatment. However, both the low and high doses of ROF treatments significantly lowered the phosphorylation levels of JAK2, JAK3, STAT1, and STAT3 (Figure 7C). These findings suggested that ROF has the capacity to dramatically control the JAKs/STATs signaling pathway, as predicted by bioinformatics analysis.

3.8. ROF Suppressed Primary $CD4^+$ T Cells Differentiation into Th1/Th17 Cells via JAKs/STATs Signaling Pathways *in Vitro*. The STAT family of transcription factors, which are activated by JAKs, has been identified as playing a crucial role in the differentiation of Th cells.[33] Consequently, this study aimed to investigate whether ROF influences the differentiation of Th cells through the inhibition of JAK/STAT signaling pathways. Additionally, TOF, known to inhibit JAK1, JAK3, and to a lesser extent JAK2, has been reported to directly impede JAKs activation and downregulate the expression of components of the JAK-STAT pathway in a cytokine- and cell population-specific manner, both *in vitro* and *in vivo*.[34] Therefore, the TOF was utilized as a positive control to assess the modulatory effects of the ROF on the JAKs/STATs signaling pathways.

In order to assess the toxicity of ROF on cultured $CD4^+$ T cells, we first separated naïve $CD4^+$ T cells from the spleen of normal male C57BL/6J mice (Figure 8A). The study found that a 24 h ROF treatment had no effect on $CD4^+$ T cell viability at different doses (up to 20 μM) (Figure 8B). To

https://doi.org/10.1021/acsomega.4c07915
ACS Omega 2024, 9, 43233−43251

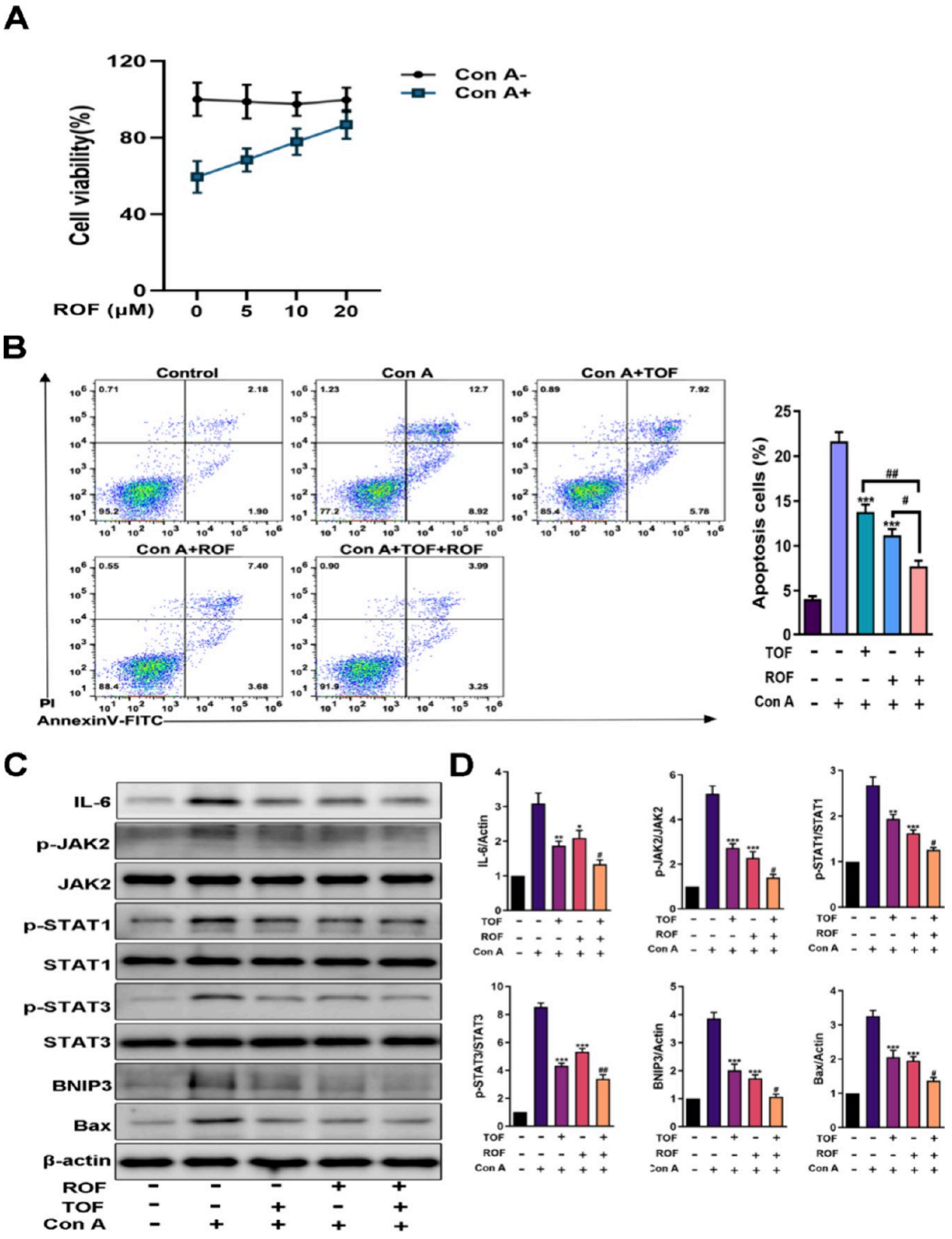

Figure 9. Effects of ROF on primary hepatocytes apoptosis *in vitro* (A) Primary hepatocytes were pretreated with ROF (5, 10, 20 μM) for 6 h and treated with or without Con A (10 μg/mL) for 24 h, the cell viability of each group was analyzed by CCK-8 assay. (B) Flow cytometry analysis of apoptosis in primary hepatocytes. (C) Primary hepatocytes were pretreated with ROF (20 μM), TOF (1 μM), or ROF (20 μM) + TOF (1 μM) for 6 h, and subsequently triggered with Con A (10 μg/mL) for 24 h. The IL-6, p-JAK2, p-STAT1, p-STAT3, BNIP3, and Bax expression levels were evaluated by using Western blotting. (D) The quantification and standardization of the protein expression were performed using ImageJ. The results are presented as mean ± SEM of three independent experiments. $^{**}P < 0.01$, $^{***}P < 0.001$ vs the Con A group. $^{\#}P < 0.05$, $^{\#\#}P < 0.01$ vs the ROF only group or TOF only group.

determine whether ROF directly affected the JAKs/STATs signaling pathways in CD4$^+$ T cells, we measured the protein expression levels of the signaling molecules in CD4$^+$ T cells stimulated with Con A. Notably, the findings indicated that nontoxic dose of ROF (20 μM) significantly reduced the phosphorylated protein levels of JAK2, JAK3, STAT1, and STAT3 in comparison to the Con A group. Simultaneously, it was noted that the combination of ROF and TOF augmented the inhibitory impact of ROF on the JAKs/STATs signaling pathways (Figure 8C,D). Subsequently, CD4$^+$ T cells were cultured under Th1 or Th17 polarization conditions to investigate the direct influence of the ROF on Th1 and Th17 subtypes. The ELISA test results indicated a significant reduction in IFN-γ and IL-17 generation in the cell supernatants of the ROF, TOF, or ROF+TOF treatment groups compared with the Con A group (Figure 8E). Furthermore, the gene expression levels of particular transcription factors involved in Th1/Th17 differentiation,

https://doi.org/10.1021/acsomega.4c07915
ACS Omega 2024, 9, 43233−43251

including *T-bet* and *RORγt*, were assessed using PCR. As depicted in Figure 8F, significant suppression of *RORγt* and *T-bet* mRNA expression was observed in cells treated with ROF, TOF, and ROF+TOF. Additionally, TOF enhanced the restraining effectiveness of ROF on the differentiation of Th1 and Th17 cells. These data align with the findings of *in vivo* experiments, suggesting that ROF can modulate Th1/Th17 cell subsets both *in vivo* and *in vitro*, partly via JAK2/3-STAT1/3 signaling pathways.

3.9. ROF Inhibited Con A-Induced Primary Hepatocytes Apoptosis via JAK2/STAT1/STAT3/BNIP3 Signaling Pathways *in Vitro*. In primary mouse hepatocytes, we also initially examined the impact of the ROF on both toxicity and proliferation. The CCK-8 assay was used to measure cell proliferation. The results exhibited that the proliferation rate of primary hepatocytes treated with ROF with escalating concentrations (0−20 μM) prior to Con A administration was progressively enhanced in a dose-dependent manner (Figure 9A). Flow cytometry analysis revealed an upregulation of apoptosis subsequent to Con A administration, while pretreatment with ROF or TOF mitigated this impact (Figure 9B), suggesting a protective role of ROF against Con A-induced hepatocytes apoptosis. Subsequently, the expression levels of IL-6, JAK2, p-STAT1, p-STAT3, and BNIP3 were assessed through Western blot analysis (Figure 9C,D). The results demonstrated elevated production of IL-6, p-JAK2, p-STAT1, p-STAT3, and BNIP3 in the Con A group, which was switched by pretreatment with ROF or TOF, suggesting that the mechanisms of action of ROF against Con A-induced hepatocyte damage partly involve the modulation of the IL-6/JAK2/STAT1/3/BNIP3 pathways.

4. DISCUSSION

The liver serves as the largest organ responsible for detoxification and anti-inflammatory responses owing to its various metabolic functions. The natural compound ROF is similarly recognized for its antitoxic and anti-inflammatory biological activities, paralleling those of the liver. Prior research has demonstrated that ROF effectively inhibits the TLR4/NF-κB signaling transduction, thereby mitigating alcoholic liver disease in mice.[21] Consequently, we posited that the ROF may reduce the pathological alterations associated with immune-mediated liver injury and enhance clinical symptoms. In the current study, we present what is, to the best of our knowledge, the first evidence indicating that ROF can provide therapeutic benefits in T cell-mediated hepatitis induced by Con A *in vivo*.

The mouse acute hepatitis induced by Con A is a broadly recognized model for studying the immune-mediated hepatitis in humans and for assessing the effectiveness of potential hepatoprotective drugs.[35] The induction of AIH by Con A is an effective method for studying the immune and inflammatory response linked to significant hepatic damage in mice within 8−12 h following a single Con A dose.[30] Based on our findings, the injection of Con A caused significant liver damage, as evidenced by elevated levels of serum biochemical indices (Figure 3B). This was additionally corroborated through the exacerbated hepatic histopathology lesions (Figure 4A). Moreover, Con A-injection led to the infiltration of neutrophils and $CD4^+$ T cells in hepatic tissues or spleens (Figure 4A). Significantly, the ROF pretreatment effectively reversed all of the biochemical and histopathological changes induced by Con A, resulting in a notable improvement in hepatic function. Additionally, in the survival assay, a high dose of ROF significantly increased the survival rates in response to Con A-induced mortality (Figure 3A). These results suggest the strong hepatoprotective activity of ROF.

Liver damage in Con A-induced hepatitis is mainly caused by the inflammatory response, which is fueled by proinflammatory Th cytokines. For instance, it has been demonstrated that elevated levels of Th1 proinflammatory cytokines, such as TNF-α and IFN-γ, accelerate the course of this illness.[32] Research has verified that IFN-γ is significantly involved in the advanced of Con A-induced hepatitis through the induction of hepatic cell apoptosis via STAT1 activation, whereas the IFN-γ deficient mice do not exhibit apoptotic cell death in liver.[36] IFN-γ can also stimulate the polarization of macrophages into pro-inflammatory M1 subtypes and enhance the production of IL-6 in activated macrophages. Studies have demonstrated that IL-6 plays a crucial role in the formation of $CD4^+$ T cells memory, supporting the proliferation and survival of $CD4^+$ T cells, and is essential for the polarization of Th17 cells.[37] Inhibiting IL-6 has been certified to effectively attenuate the hepatic damage in Con A-induced AIH model.[30] Besides, Con A triggers an excessive production of TNF-α, leading to the increased release of other cytokines, heightened expression of adhesion molecules, and intensified inflammatory response in cases of hepatitis. The interaction between TNF-α and tumor necrosis factor receptor-1 (TNFR1) is essential for triggering downstream processes and enabling the transmission of signals that ultimately result in hepatic apoptosis.[38] Additionally, IL-2 is also a major cytokine secreted by Th1 cells and has been identified as a crucial factor in the growth of lymphocytes during adaptive immune responses,[39] such as AIH.[40] Furthermore, Th17 cells are significantly involved in the pathogenesis of AIH. These cells are characterized by the expression of the proinflammatory cytokine IL-17 and are capable of secreting additional cytokines, including IL-6, IL-21, and IL-22.[41] Particularly, the cytokine IL-17 has been shown to facilitate the migration of neutrophils and monocytes to the site of inflammation, which contributes to the promotion of inflammation and induces hepatocyte apoptosis and necrosis.[42] Therefore, the targeting of proinflammatory cytokines produced by $CD4^+$ T cells, specifically those associated with the Th1 and Th17 subtypes, may represent a promising therapeutic strategy for AIH. In the present investigation, our findings demonstrated that ROF effectively inhibited immune responses by suppressing the production of TNF-α and IFN-γ, as evidenced by our ELISA and PCR experiments conducted on circulating or hepatic tissues (Figure 5A,B). We also noted that the elevation of IL-2 levels in serum was not substantial (Figure 5A). This phenomenon may be attributed to the kinetics of IL-2 in Con A-induced AIH in mice, where IL-2 levels peak approximately 2−4 h postinduction and subsequently decline rapidly.[35] Nevertheless, the administration of the ROF treatment also resulted in a partial inhibition of IL-2 expression across the various groups. Additionally, our flow cytometric analysis of hepatic $CD4^+$ T cells and Th1 polarization experiments in isolated $CD4^+$ T cells all revealed that ROF could directly inhibit Th1 subtypes *in vivo* and *in vitro* (Figure 5C, Figure 8E,F). Furthermore, although other studies have shown that circulating IL-17 levels do not increase after Con A injection,[43] our results revealed a significant elevation in *IL-17* gene expression in hepatic tissues (Figure 5B), as reported by a previous study.[11] Concurrently, the mRNA expression level of *IL-6* in liver tissue was notably reduced by ROF. On the other hand, the Th17 subtypes in

https://doi.org/10.1021/acsomega.4c07915
ACS Omega 2024, 9, 43233−43251

hepatic $CD4^+$ T cells or primary $CD4^+$ T cells were also significantly upregulated following Con A injection or under the condition of Th17 polarization (Figure 5C, Figure 8E,F). However, the ROF treatment effectively reduced Th17 subtypes and the generation of proinflammatory factors. These findings indicated that ROF has a crucial impact on the functioning of Th1 and Th17 cells in the Con A induced AIH model and purified $CD4^+$ T cells. The results of these *in vivo* and *in vitro* experiments are consistent with our predictions made using bioinformatics analysis, which showed that the ROF may influence the differentiation of Th cells. Altogether, these data uncovered that the ROF possessed valuable modulatory effects on $CD4^+$ T cells, particularly on Th1 and Th17 cells. Beyond that, there is a significant presence of NKT cells that release a cascade of Th1 and Th2 type cytokines such as IL-4 and IFN-γ during the inflammatory response in AIH.[44] NKT cells are also actively involved in the direct engagement of perforin/granzyme and/or Fas/Fas ligand (FasL) pathways to carry out cytotoxic functions, which further induce the hepatic damage.[45] Our bioinformatics analysis findings indicated that ROF may also be involved in the toxicity regulated by NKT cells (Figure 1D). Therefore, the underlying mechanism of whether ROF protected Con A triggered hepatic damage through modulating the functions of NKT cells needs to be investigated in further studies.

The JAK-STAT signaling pathways consist of four Janus kinases: JAK1, JAK2, JAK3, and tyrosine kinase 2, as well as several STATs, specifically STAT1 through STAT6.[34] Numerous studies have reported that the JAKs/STATs signaling pathways have significantly taken part in the proliferation and differentiation of several effector T cells and have emerged as a crucial focus for combating T-cell related inflammatory conditions *in vivo*.[46] When a cytokine binds to its corresponding receptor, it triggers the JAK-STAT signaling cascade. This process promotes the activation of JAK through trans-phosphorylation, which in turn stimulates the transcription of STATs.[46] For instance, signaling of IL-6 through JAK2, which modulates STAT3 activity, is important for the differentiation of Th17 cells. Analogously, IFN-γ signaling through JAK2/STAT1 or IL-12 signaling through JAK2/STAT4 is significant for the differentiation of Th1 cells.[47] Furthermore, JAK3 is associated with multiple cytokine pathways, playing a crucial role in initiating signaling for interleukins, such as IL-2, IL-4, IL-7, IL-9, IL-13, and IL-15. It modulates the transcriptional activity and functionality of STAT1, STAT3, and STAT5 within T cells, is involved in T cell activation and proliferation, and significantly contributes to the pathological mechanisms underlying inflammatory diseases resulting from autoimmunity or transplantation.[13] In our bioinformatics analysis, we identified JAK2 and JAK3 as the important targets for ROF in enhancing AIH. Via molecular docking and dynamic simulations, we found that ROF exhibited a strong and stable binding affinity with both JAK2 and JAK3. It is widely acknowledged that the accuracy of simulation results was not only affected by the simulation time and molecular structure but may also vary due to factors such as the choice of simulation software and the settings of simulation parameters. As a result, we performed pertinent validations at both animal and cellular levels. Through IHC and Western blotting, we have verified that ROF can markedly reduce the phosphorylated JAK2, JAK3, STAT1, and STAT3 protein levels in the hepatic tissues of the AIH model (Figure 7A−C). In experiments involving *in vitro* T cell polarization, we additionally confirmed that the ROF has the capacity to directly impact the JAK2/JAK3/STAT1/STAT3 signaling pathways, thereby impeding the differentiation of Th1 and Th17 cells (Figure 8C). In summary, these data demonstrated that ROF may partially attenuate Con A-induced hepatic damage by regulating the JAKs/STATs signaling pathway-mediated T cell polarization. In the future, further research is required to explore the regulatory effects of ROF on T cell development, activation, proliferation, and its distinct functional subtypes, including Treg cells. This exploration is essential to uncover the potential of ROF in enhancing the management of T cell-mediated immune inflammatory conditions.

As mentioned above, the JAKs/STATs signaling transduction has been confirmed to be closely connected with the mechanisms underlying hepatocyte apoptosis in the AIH model, in addition to its role in regulating immune processes. For instance, a prior study confirmed that arctigenin mitigated hepatocyte apoptosis through restraining of the IFN-γ/IL-6/JAKs/STAT1 signaling pathways.[14] Moreover, gastrodin pretreatment inhibited the IL-6/JAK2/STAT3 signaling pathway, demonstrating protective benefits against hepatic apoptosis caused by Con A.[15] Other studies have validated that epigallocatechin-3-gallate displayed antiapoptotic effects in hepatic cells via restricting BNIP3 activity through the IL-6/JAKs/STAT3 pathways.[16] Thus, we further evaluated the antiapoptotic effects of ROF both *in vivo* and *in vitro*. IHC and Western blotting results suggest that in the AIH model, ROF can significantly inhibit the generation of proapoptotic proteins including cleaved-caspase-3, cleaved-caspase-9, and Bax while promoting the antiapoptotic protein Bcl-2 production (Figure 6A,B). *In vitro*, in Con A-induced primary hepatocytes, CCK-8 and flow cytometry results pointed out that ROF can dose-dependently improve the occurrence of cell apoptosis (Figure 9A,B). Moreover, mechanistic studies showed that ROF could significantly regulate the IL-6/JAK2/STAT1/3/BNIP3 signaling molecules (Figure 9C). However, we did not investigate the expression of the JAK3 protein because JAK3 is primarily expressed at high levels in hematopoietic cells, whereas the other members of JAKs are widely expressed in various tissues.[48] In addition, studies have documented that STAT1/STAT3 could also regulate hepatic autophagy via BNIP3 processes to interact with apoptosis in hepatocyte cells.[49] In our upcoming experiments, it is important to investigate whether ROF regulates autophagy in the AIH model, thereby influencing apoptosis and ameliorating hepatic injury.

As we all know, drug development frequently encounters substantial challenges, including inadequate pharmacokinetic properties and low *in vivo* activity. The pharmacokinetic study of ROF after intravenous administration (1 mg/kg) in rats have been evaluated by Liu et al. Their data showed that ROF eliminated quickly and the elimination half-life ($T_{1/2}$) value was 1.20 ± 0.29 h.[50] Through predictions and evaluations using the SwissADME database (http://www.swissadme.ch/), we found that ROF has low gastrointestinal (GI) absorption, with a bioavailability score of 0.17. Therefore, despite ROF exhibiting various biological activities, its clinical application may be constrained by limited bioavailability and a rapid release rate. Research conducted by Al-Shalabi et al. demonstrated that ROF loaded in poly(lactide-*co*-glycolide) (PLGA) nanoparticles (NPs) displayed a superior antioxidant stress effect in RAW264.7 cells when compared to ROF. Furthermore, in a formalin-induced rat paw edema model,

https://doi.org/10.1021/acsomega.4c07915
ACS Omega 2024, 9, 43233−43251

ROF-NPs were shown to more effectively ameliorate pathological changes and the inflammatory response in foot tissue.[51] Hence, focused endeavors on preparing and screening suitable ROF-NPs to enhance their *in vivo* activity for precisely targeting T cell-mediated inflammatory disease, such as AIH, are crucial for the future clinical application of ROF.

5. CONCLUSION

In summary, ROF effectively provided protection against Con A-induced AIH by lowering the invasion of immune cells, impairing caspase-dependent apoptosis, and suppressing Th1/Th17 cells function. ROF could also attenuate the proinflammatory cytokines secretion and downregulate the JAKs/STATs signaling molecules in both $CD4^+$ T cells and primary hepatocytes. This research may represent the initial comprehensive exploration of the molecular and pharmacological mechanisms underlying the potential therapeutic effects of ROF in addressing AIH. The characteristic and specific modulatory actions of ROF result in its extended ability to combat this type of hepatitis through its anti-inflammatory, antiapoptotic, and immunoregulatory properties. This research offers a theoretical framework for the advancement of ROF as a potent treatment for hepatic disorders mediated by T cells. Additional investigation is required to delineate the ameliorative efficacy of ROF against AIH and to assess its suitability for possible clinical use.

AUTHOR INFORMATION

Corresponding Authors

Nan Zeng − *State Key Laboratory of Southwestern Chinese Medicine Resources, School of Pharmacy, Chengdu University of Traditional Chinese Medicine, Chengdu, Sichuan 611137, P. R. China*; orcid.org/0000-0003-2090-4288; Phone: +86-13198502352; Email: 19932015@cdutcm.edu.cn; Fax: +86-28-6180-0231

Yue Tong − *Department of Gastroenterology, Xinqiao Hospital, Third Military Medical University (Army Medical University), Chongqing 400037, P. R. China*; Phone: +86-13134351112; Email: tong1231@tmmu.edu.cn; Fax: +86-23-6875-5114

Authors

Ge Zhao − *Department of Pharmacy, The Affiliated Hospital, Southwest Medical University, Luzhou, Sichuan 646000, P. R. China; State Key Laboratory of Southwestern Chinese Medicine Resources, School of Pharmacy, Chengdu University of Traditional Chinese Medicine, Chengdu, Sichuan 611137, P. R. China*; orcid.org/0000-0001-9561-2971

Hu Qi − *State Key Laboratory of Southwestern Chinese Medicine Resources, School of Pharmacy, Chengdu University of Traditional Chinese Medicine, Chengdu, Sichuan 611137, P. R. China*

Minghua Liu − *Department of Pharmacology, School of Pharmacy, Southwest Medical University, Luzhou, Sichuan 646000, P. R. China*

Ting Zhou − *State Key Laboratory of Southwestern Chinese Medicine Resources, School of Pharmacy, Chengdu University of Traditional Chinese Medicine, Chengdu, Sichuan 611137, P. R. China*

Li Chen − *Department of Pharmacy, Clinical Medical College and The First Affiliated Hospital of Chengdu Medical College, Chengdu, Sichuan 610500, P. R. China*

Chunhong Wu − *Information Centre, Chengdu University, Chengdu, Sichuan 610106, P. R. China*

Xiongwei Zhang − *State Key Laboratory of Southwestern Chinese Medicine Resources, School of Pharmacy, Chengdu University of Traditional Chinese Medicine, Chengdu, Sichuan 611137, P. R. China*

Complete contact information is available at: https://pubs.acs.org/10.1021/acsomega.4c07915

Author Contributions

G.Z.: conceptualization, investigation, methodology, writing—original draft, writing—review and editing. H.Q.: methodology, investigation. M.L.: methodology, validation. T.Z.: methodology, validation. L.C.: methodology, investigation. C.W.: methodology, validation. X.Z.: methodology, investigation. N.Z.: funding acquisition, conceptualization, validation, writing—review and editing. Y.T.: methodology, investigation, validation, writing—review and editing. All authors have reviewed and endorsed the final draft of the manuscript for publication.

Notes

The authors declare no competing financial interest.

ACKNOWLEDGMENTS

Funding for this investigation was provided by the Chinese National Natural Science Foundation (Grant 82074094).

REFERENCES

(1) Mu, M.; Zhang, Z. W.; Cheng, Y.; Liu, G. Z.; Chen, X. S.; Wu, X.; Zhuang, C. F.; Liu, B. Y.; Kong, X. P.; You, S. Augmenter of liver regeneration (ALR) restrains concanavalin A-induced hepatitis in mice. *Int. Immunopharmacol.* **2016**, *35*, 280−286.

(2) Que, W. C.; Lin, H. L.; Li, X. Y.; Zhang, B. Q.; Liu, M. B.; Hu, X.; Fu, J. S.; Cheng, Y.; Qiu, H. Q. Koumine ameliorates concanavalin A-induced autoimmune hepatitis in mice: involvement of the Nrf2, NF-κB pathways, and gut microbiota. *Int. Immunopharmacol.* **2023**, *114*, No. 109573.

(3) Bunchorntavakul, C.; Reddy, K. R. Acetaminophen (APAP or N-Acetyl-p-Aminophenol) and Acute Liver Failure. *Clin Liver Dis.* **2018**, *22* (2), 325−346.

(4) Manns, M. P.; Lohse, A. W.; Vergani, D. Autoimmune hepatitis–Update 2015. *J. Hepatol.* **2015**, *62* (1, Suppl.), S100−S111.

(5) Terziroli Beretta-Piccoli, B.; Mieli-Vergani, G.; Vergani, D. Autoimmune hepatitis: Standard treatment and systematic review of alternative treatments. *World J. Gastroenterol.* **2017**, *23* (33), 6030−6048.

(6) Sapisochin, G.; Bruix, J. Liver transplantation for hepatocellular carcinoma: outcomes and novel surgical approaches. *Nat. Rev. Gastroenterol Hepatol.* **2017**, *14* (4), 203−217.

(7) Zhang, Y.; Li, S. N.; He, L.; Wang, F.; Chen, K.; Li, J. J.; Liu, T.; Zheng, Y. Y.; Wang, J. R.; Lu, W. X.; Zhou, Y. Q.; Yin, Q.; Xia, Y. J.; Zhou, Y. Q.; Lu, J.; Guo, C. Y. Combination therapy of fenofibrate and ursodeoxycholic acid in patients with primary biliary cirrhosis who respond incompletely to UDCA monotherapy: a meta-analysis. *Drug Des Devel Ther.* **2015**, *9*, 2757−66.

(8) Heymann, F.; Hamesch, K.; Weiskirchen, R.; Tacke, F. The concanavalin A model of acute hepatitis in mice. *Lab. Anim.* **2015**, *49* (1 Suppl.), 12−20.

(9) Zhuang, Y.; Li, Y.; Li, X. F.; Xie, Q.; Wu, M. Atg7 Knockdown Augments Concanavalin A-Induced Acute Hepatitis through an ROS-Mediated p38/MAPK Pathway. *PLoS One.* **2016**, *11* (3), No. e0149754.

(10) Liu, Y.; Hao, H.; Hou, T. Concanavalin A-induced autoimmune hepatitis model in mice: Mechanisms and future outlook. *Open Life Sci.* **2022**, *17* (1), 91−101.

(11) Chen, F. Y.; Zhou, L. F.; Li, X. Y.; Zhao, J. W.; Xu, S. F.; Huang, W. H.; Gao, L. J.; Hao, S. J.; Ye, Y. P.; Sun, H. X. Stephanthraniline A suppressed CD4(+) T cell-mediated immunological hepatitis through impairing PKCθ function. *Eur. J. Pharmacol.* **2016**, *789*, 370−384.
(12) Xue, C.; Yao, Q.; Gu, X.; Shi, Q.; Yuan, X.; Chu, Q.; Bao, Z.; Lu, J.; Li, L. Evolving cognition of the JAK-STAT signaling pathway: autoimmune disorders and cancer. *Signal Transduction Targeted Ther.* **2023**, *8* (1), 204.
(13) Hu, X.; Li, J.; Fu, M.; Zhao, X.; Wang, W. The JAK/STAT signaling pathway: from bench to clinic. *Signal Transduction Targeted Ther.* **2021**, *6* (1), 402.
(14) Feng, Q.; Yao, J.; Zhou, G.; Xia, W.; Lyu, J.; Li, X.; Zhao, T.; Zhang, G.; Zhao, N.; Yang, J. Quantitative Proteomic Analysis Reveals That Arctigenin Alleviates Concanavalin A-Induced Hepatitis Through Suppressing Immune System and Regulating Autophagy. *Front. Immunol.* **2018**, *9*, 1881.
(15) Zhou, Y.; Chen, J.; Yao, Z.; Gu, X. Gastrodin ameliorates Concanavalin A-induced acute hepatitis via the IL6/JAK2/STAT3 pathway. *Immunopharmacol Immunotoxicol.* **2022**, *44* (6), 925−934.
(16) Li, S.; Xia, Y.; Chen, K.; Li, J.; Liu, T.; Wang, F.; Lu, J.; Zhou, Y.; Guo, C. Epigallocatechin-3-gallate attenuates apoptosis and autophagy in concanavalin A-induced hepatitis by inhibiting BNIP3. *Drug Des Devel Ther.* **2016**, *10*, 631−47.
(17) Brinza, I.; Abd-Alkhalek, A. M.; El-Raey, M. A.; Boiangiu, R. S.; Eldahshan, O. A.; Hritcu, L. Ameliorative Effects of Rhoifolin in Scopolamine-Induced Amnesic Zebrafish (Danio rerio) Model. *Antioxidants (Basel).* **2020**, *9* (7), 580.
(18) Gattuso, G.; Barreca, D.; Gargiulli, C.; Leuzzi, U.; Caristi, C. Flavonoid composition of Citrus juices. *Molecules.* **2007**, *12* (8), 1641−73.
(19) Zheng, B.; Zheng, Y.; Zhang, N.; Zhang, Y.; Zheng, B. Rhoifolin from Plumula Nelumbinis exhibits anti-cancer effects in pancreatic cancer via AKT/JNK signaling pathways. *Sci. Rep.* **2022**, *12* (1), 5654.
(20) Liao, S.; Song, F.; Feng, W.; Ding, X.; Yao, J.; Song, H.; Liu, Y.; Ma, S.; Wang, Z.; Lin, X.; Xu, J.; Zhao, J.; Liu, Q. Rhoifolin ameliorates titanium particle-stimulated osteolysis and attenuates osteoclastogenesis via RANKL-induced NF-κB and MAPK pathways. *J. Cell Physiol.* **2019**, *234* (10), 17600−17611.
(21) Mai, B.; Han, L.; Zhong, J.; Shu, J.; Cao, Z.; Fang, J.; Zhang, X.; Gao, Z.; Xiao, F. Rhoifolin Alleviates Alcoholic Liver Disease In Vivo and In Vitro via Inhibition of the TLR4/NF-κB Signaling Pathway. *Front Pharmacol.* **2022**, *13*, No. 878898.
(22) Liu, L.; Liang, L.; Yang, C.; Chen, Y. Machine learning-based solution reveals cuproptosis features in inflammatory bowel disease. *Front. Immunol.* **2023**, *14*, No. 1136991.
(23) Wang, M. H.; Yin, H. L.; Xia, Y.; Tu, Y. J.; Zou, X. S.; Song, W. C.; Luo, L. C.; Wu, H. Z.; Yang, Y. F.; Zan, J. F.; Liu, Y. W.; Dan, H. X.; Yin, Q.; You, P. Huganbuzure Granule Attenuates Concanavalin-A-Induced Immune Liver Injury in Mice via Regulating the Balance of Th1/Th2/Th17/Treg Cells and Inhibiting Apoptosis. *Evidence-Based Complementary Altern. Med.* **2021**, *2021*, No. 5578021.
(24) El-Agamy, D. S. Pirfenidone ameliorates concanavalin A-induced hepatitis in mice via modulation of reactive oxygen species/nuclear factor kappa B signalling pathways. *J. Pharm. Pharmacol.* **2016**, *68* (12), 1559−1566.
(25) Watarai, H.; Nakagawa, R.; Omori-Miyake, M.; Dashtsoodol, N.; Taniguchi, M. Methods for detection, isolation and culture of mouse and human invariant NKT cells. *Nat. Protoc.* **2008**, *3* (1), 70−8.
(26) Tao, Y. Y.; Yan, X. C.; Zhou, T.; Shen, L.; Liu, Z. L.; Liu, C. H. Fuzheng Huayu recipe alleviates hepatic fibrosis via inhibiting TNF-α induced hepatocyte apoptosis. *BMC Complementary Altern. Med.* **2014**, *14*, 449.
(27) Zhu, J.; Yamane, H.; Paul, W. E. Differentiation of effector CD4 T cell populations (*). *Annu. Rev. Immunol.* **2010**, *28*, 445−89.
(28) Li, R.; Zhu, L.; Wu, M.; et al. Serum Pharmacochemistry Combined with Network Pharmacology-Based Mechanism Prediction and Pharmacological Validation of Zhenwu Decoction on Alleviating Isoprenaline-Induced Heart Failure Injury in Rats. *ACS Omega.* **2023**, *8* (40), 37233−37247.
(29) Mahdi, I.; Yeasmin, H.; Hossain, I.; et al. Potential antiviral peptides against the nucleoprotein of SARS-CoV-2. *Chem. Zvesti.* **2023**, *77* (2), 813−823.
(30) El-Agamy, D. S.; Shaaban, A. A.; Almaramhy, H. H.; Elkablawy, S.; Elkablawy, M. A. Pristimerin as a Novel Hepatoprotective Agent Against Experimental Autoimmune Hepatitis. *Front. Pharmacol.* **2018**, *9*, 292.
(31) Que, W. C.; Lin, H. L.; Li, X. Y.; Zhang, B. Q.; Liu, M. B.; Hu, X.; Fu, J. S.; Cheng, Y.; Qiu, H. Q. Koumine ameliorates concanavalin A-induced autoimmune hepatitis in mice: involvement of the Nrf2, NF-κB pathways, and gut microbiota. *Int. Immunopharmacol.* **2023**, *114*, No. 109573.
(32) Zhou, Y. Q.; Weng, X. F.; Dou, R.; Tan, X. S.; Zhang, T. T.; Fang, J. B.; Wu, X. W. Betulin from Hedyotis hedyotidea ameliorates concanavalin A-induced and T cell-mediated autoimmune hepatitis in mice. *Acta Pharmacol Sin.* **2017**, *38* (2), 201−210.
(33) O'Shea, J. J.; Plenge, R. JAK and STAT signaling molecules in immunoregulation and immune-mediated disease. *Immunity.* **2012**, *36* (4), 542−550.
(34) Palmroth, M.; Kuuliala, K.; Peltomaa, R.; et al. Tofacitinib Suppresses Several JAK-STAT Pathways in Rheumatoid Arthritis In Vivo and Baseline Signaling Profile Associates With Treatment Response. *Front Immunol.* **2021**, *12*, No. 738481.
(35) Wang, H. X.; Liu, M.; Weng, S. Y.; Li, J. J.; Xie, C.; He, H. L.; Guan, W.; Yuan, Y. S.; Gao, J. Immune mechanisms of Concanavalin A model of autoimmune hepatitis. *World J. Gastroenterol.* **2012**, *18* (2), 119−25.
(36) Tagawa, Y.; Sekikawa, K.; Iwakura, Y. Suppression of concanavalin A-induced hepatitis in IFN-gamma(-/-) mice, but not in TNF-alpha(-/-) mice: role for IFN-gamma in activating apoptosis of hepatocytes. *J. Immunol.* **1997**, *159* (3), 1418−28.
(37) Manku, S.; Wong, W.; Luo, Z.; et al. IL-6 expression is correlated with increased T-cell proliferation and survival in the arterial wall in giant cell arteritis. *Cardiovasc Pathol.* **2018**, *33*, 55−61.
(38) Wang, K.; Song, Z.; Wang, H.; Li, Q.; Cui, Z.; Zhang, Y. Angelica sinensis polysaccharide attenuates concanavalin A-induced liver injury in mice. *Int. Immunopharmacol.* **2016**, *31*, 140−8.
(39) Zhao, G.; Tong, Y.; Xu, J.; et al. Jing-Fang powder ethyl acetate extracts attenuate atopic dermatitis by modulating T-cell activity. *Mol. Immunol.* **2023**, *160*, 133−149.
(40) Sass, G.; Heinlein, S.; Agli, A.; Bang, R.; Schümann, J.; Tiegs, G. Cytokine expression in three mouse models of experimental hepatitis. *Cytokine.* **2002**, *19* (3), 115−120.
(41) Ji, W.; Peng, X.; Lou, T.; Wang, J.; Qiu, W. Total flavonoids from Tetrastigma hemsleyanum ameliorates inflammatory stress in concanavalin A-induced autoimmune hepatitis mice by regulating Treg/Th17 immune homeostasis. *Inflammopharmacology.* **2019**, *27* (6), 1297−1307.
(42) Liu, T.; Zhang, L.; Joo, D.; Sun, S. C. Nf-Kb signaling in infammation. *Signal Transduction Targeted Ther.* **2017**, *2*, No. 17023.
(43) Ye, X. J.; Xu, R.; Liu, S. Y.; Hu, B.; Shi, Z. J.; Shi, F. L.; Zeng, B.; Xu, L. H.; Huang, Y. T.; Chen, M. Y.; Zha, Q. B.; He, X. H.; Ouyang, D. Y. Taraxasterol mitigates Con A-induced hepatitis in mice by suppressing interleukin-2 expression and its signaling in T lymphocytes. *Int. Immunopharmacol.* **2022**, *102*, No. 108380.
(44) Kumar, V. NKT-cell subsets: promoters and protectors in inflammatory liver disease. *J. Hepatol.* **2013**, *59* (3), 618−20.
(45) Takeda, K.; Hayakawa, Y.; Van Kaer, L.; Matsuda, H.; Yagita, H.; Okumura, K. Critical contribution of liver natural killer T cells to a murine model of hepatitis. *Proc. Natl. Acad. Sci. U. S. A.* **2000**, *97* (10), 5498−503.
(46) Seif, F.; Khoshmirsafa, M.; Aazami, H.; Mohsenzadegan, M.; Sedighi, G.; Bahar, M. The role of JAK-STAT signaling pathway and its regulators in the fate of T helper cells. *Cell Commun. Signaling* **2017**, *15* (1), 23.

https://doi.org/10.1021/acsomega.4c07915
ACS Omega 2024, 9, 43233−43251

(47) Meitei, H. T.; Lal, G. T cell receptor signaling in the differentiation and plasticity of CD4+ T cells. *Cytokine Growth Factor Rev.* **2023**, *69*, 14−27.
(48) Degryse, S.; de Bock, C. E.; Cox, L.; Demeyer, S.; Gielen, O.; Mentens, N.; Jacobs, K.; Geerdens, E.; Gianfelici, V.; Hulselmans, G.; Fiers, M.; Aerts, S.; Meijerink, J. P.; Tousseyn, T.; Cools, J. JAK3 mutants transform hematopoietic cells through JAK1 activation, causing T-cell acute lymphoblastic leukemia in a mouse model. *Blood.* **2014**, *124* (20), 3092−100.
(49) Delgado, M.; Tesfaigzi, Y. BH3-only proteins, Bmf and Bim, in autophagy. *Cell Cycle.* **2013**, *12* (22), 3453−4.
(50) Liu, H.; Xu, C.; Wang, W.; Zhao, Y. Development and Validation of an LC-ESI-MS/MS Method for Simultaneous Determination of Ligustroflavone and Rhoifolin in Rat Plasma and Its Application to a Pharmacokinetic Study. *J. Chromatogr Sci.* **2017**, *55* (3), 267−274.
(51) Al-Shalabi, E.; Abusulieh, S.; Hammad, A. M.; Sunoqrot, S. Rhoifolin loaded in PLGA nanoparticles alleviates oxidative stress and inflammation in vitro and in vivo. *Biomater Sci.* **2022**, *10* (19), 5504−5519.

https://doi.org/10.1021/acsomega.4c07915
ACS Omega 2024, 9, 43233−43251